Journal of Advanced Research (2015) 6, 643–661

Cairo University

Journal of Advanced Research

REVIEW

Advances in atomic physics Four decades of contribution of the Cairo University – Atomic Physics Group

Tharwat M. El-Sherbini *

Physics Department, Faculty of Science, Cairo University, Giza, Egypt

GRAPHICAL ABSTRACT

In this review article, important developments in the field of atomic physics are highlighted and linked to research works the author was involved in himself as a leader of the Cairo University – Atomic Physics Group. Starting from the late 1960s – when the author first engaged in research - an overview is provided of the milestones in the fascinating landscape of atomic physics.

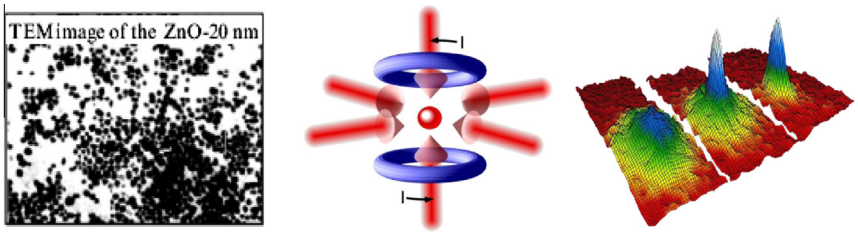

ARTICLE INFO

Article history:
Received 26 May 2013
Received in revised form 19 August 2013
Accepted 19 August 2013
Available online 26 August 2013

Keywords:
Atomic physics
Laser physics
Plasma physics
Astrophysics

ABSTRACT

In this review article, important developments in the field of atomic physics are highlighted and linked to research works the author was involved in himself as a leader of the Cairo University – Atomic Physics Group. Starting from the late 1960s – when the author first engaged in research – an overview is provided of the milestones in the fascinating landscape of atomic physics.

* Corresponding author. Tel.: +20 1002501511.
E-mail address: thelsherbini@hotmail.com.

Peer review under responsibility of Cairo University.

Production and hosting by Elsevier

http://dx.doi.org/10.1016/j.jare.2013.08.004

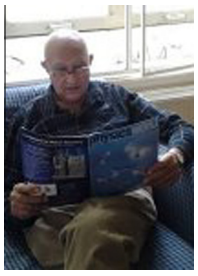

Tharwat El-Sherbini is the leader of the atomic physics group at Cairo University. He acquired a Ph. D. in atomic and molecular physics from Leiden University (The Netherlands) in 1972 and a D. Sc. degree in atomic and laser physics in 1984. He has published more than 160 publications in the field of atomic, molecular and laser physics and has established the research Laboratory of Lasers and New Materials (LLNM) at the physics department of Cairo University. Professor El-Sherbini has received several awards and honors, among which: the "State Award for Scientific Appreciation", the "NILE Award" and the "State Decoration Of The First Order For Sciences and Arts".

Introduction

During the last decades, we witnessed a continuous development in the field of atomic physics that had direct impact on other fields of research such as astrophysics, plasma physics, controlled thermonuclear fusion, laser physics, and condensed matter physics.

The landscape is vast and cannot possibly be covered in one review article, but it would require a complete book. Therefore, I will confine myself to the research works I was involved in and those that have direct connections with the work I have done.

The review is structured around five main topics:

- Electron–atom collisions.
- Ion–atom collisions.
- Atomic structure calculations and X-ray lasers.
- Laser-induced breakdown spectroscopy (LIBS).
- Laser cooling and Bose–Einstein condensation.

Electron–atom collisions

The physics of electron–atom collisions originated in 1930 by the work of Ramsauer and Kollath [1,2] on the total scattering cross-section of low energy electrons against noble gases, which contributed so much to the development of quantum theory. This work was followed by Tate and Smith [3] on inelastic total cross-sections for excitation of noble gases. Several well known physicists, e.g., Bleakney and Smith [4], Hughes and Rojansky [5], and Massey and Smith [6], at this period gave important contributions in the field of electron collision physics. The theory was developed by Stueckelberg [7], Landau [8], and Zener [9]. In 1952, Massey and Burhop's book [10] appeared on "Electronic and Ionic Impact phenomena," which provided the basis for any scientist who wants to start the work on the subject.

Multiple ionization of noble gases by low energy electrons (below 600 eV) has been studied extensively in mass spectrometers [3,11,12]. However, total electron impact cross-sections were determined by Van der Wiel et al. [13] and El-Sherbini et al. [14] for the formation of singly and multiply charged ions of He, Ne, Ar, Kr, and Xe by fast electrons (2–16 keV). The ion selection was performed in a charge analyzer with 100% transmission, and consequently, it was possible to avoid the discrimination effects in the measurement of the relative abundances of the multiply charged ions. Therefore, the data were more reliable than those obtain in low transmission mass spectrometers. The ionization cross-section of large electron impact energies is given by

$$\frac{\sigma_{ni}}{4\pi a_0^2}\frac{E_{el}}{R} = M_{ni}^2 \ln E_{el} + C_{ni} \tag{1}$$

where σ_{ni} is the cross-section for formation of $n+$ ions, E_{el} is the electron energy corrected for relativistic effects, a_0 is the first Bohr radius, R is the Rydberg energy, M_{ni}^2, and C_{ni} are constants.

The constant M_{ni}^2 is given by

$$M_{ni}^2 = \int_{n+} \frac{df^{n+}}{dE}\frac{R}{E}dE \tag{2}$$

where df^{n+}/dE is the differential dipole oscillator strength for an ionization to n^+ continuum at excitation energy E.

In 1970, an experiment was developed by van der Wiel [15], in which fast electrons (10 keV), scattered by He, Ne, and Ar are detected in coincidence with the ions formed (Fig. 1). It was possible from the measurements of the scattering intensity at small angles to calculate optical oscillator strengths. The differential scattering of fast electrons is given by Bethe et al. [16] (in au):

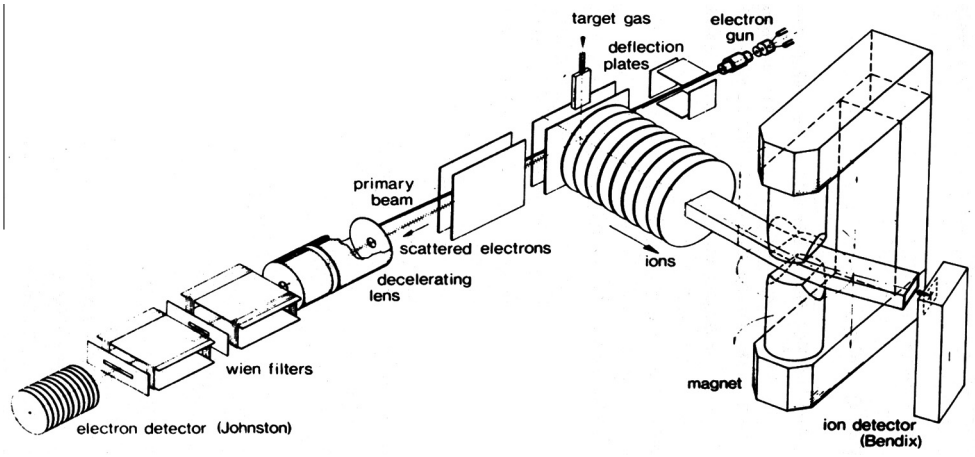

Fig. 1 Schematic view of the scattered electron–ion coincidence apparatus. **The first table-top synchrotron**.

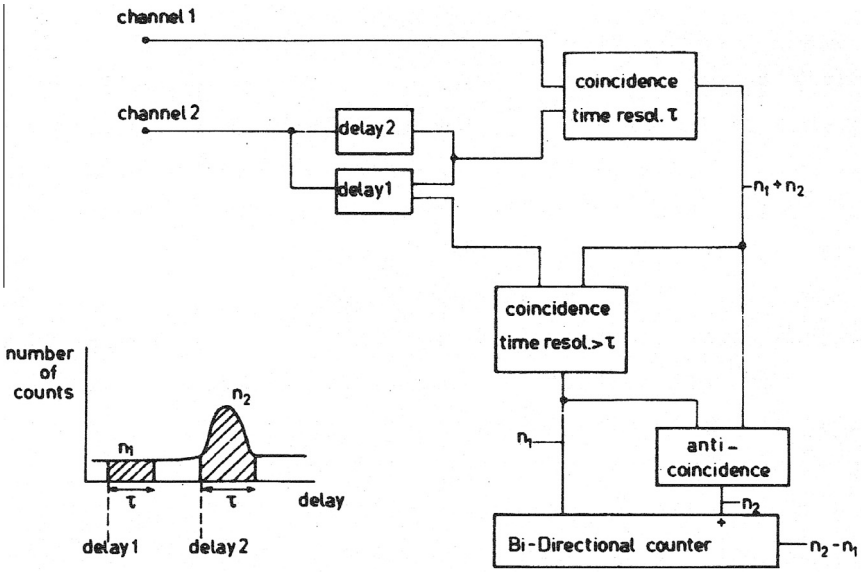

Fig. 2 Block diagram of the coincidence circuit. Signal from the ion detector (channel 1). Signal from the electron detector (channel 2).

$$\sigma(\vartheta, E) = \frac{2}{E}\frac{k_n}{k_0}\frac{1}{K^2}\frac{df(K)}{dE} \tag{3}$$

where ϑ is the scattering angle, E the energy loss, k_0 and k_n are the magnitudes of the momenta of the primary electron before and after collision, K is the magnitude of the momentum transfer ($K = k_0 - k_n$), and $(df(K)/dE)$ is the generalized oscillator strength. This last quantity may be expanded in terms of K^2:

$$\frac{df(K)}{dE} = \frac{df}{dE} + aK^2 + bK^4 + \tag{4}$$

where $\frac{df}{dE}$ is the optical oscillator strength, as defined in the dipole approximation.

The work was closely connected to that where ion charge distribution is measured after irradiation of atoms with photons at a number of selected wavelengths [17,18]. However, the use of photon source is simulated by measuring the small-angle, inelastic scatting of 10 keV electrons in coincidence with the ions formed. The simulation is based on the fact that measured energy lost by the scattered electron in the coincident experiment corresponds to the photon energy absorbed in the photon experiments for the same process. Moreover, the incident electron energy of 10 keV is large compared to the energy losses studied $\leqslant$400 eV, and also, the incident momentum (370 au) is much larger than the momentum transfer ($\leqslant$0.5 au). Under these conditions, the first Born approximation holds. By making use of the first Born approximation for inelastic electron scattering at small momentum transfer, the measured intensities of scattering were converted into optical oscillator strengths. Fig. 2 shows the block diagram of the electronic circuit, where signals from the ion and the electron detectors are measured in delayed coincidence. The true coincidences after being separated from the simultaneously registered accidental ones are stored in a data collector that drives the energy loss scanning. The number of true coincidences is recorded per number of ions of the charge state under consideration. This enables us to put spectra for different charge states on the same relative scale when knowing the relative abundances of the charge states at 10 keV electron impact energy. This technique combines the advantage of continuous variability of the energy transfer over a few hundred eV with that of a constant detection efficiency. As a result, oscillator-strength spectra over a wide energy range were obtained, which could be put on an absolute scale by normalization on an absolute photo-absorption value at only one energy. As far as the intensity is concerned, this method compares favorably with a possible alternative of charge analysis of ions formed by dispersed electron synchrotron radiation in a low density target (10^{-5} torr). This work was extended by El-Sherbini and van der Wiel [19] to measure oscillator strengths for multiple ionization in the outer and first inner shells of Kr and Xe (Figs. 3 and 4). Direct ejection of two N electrons below the $3d^9$ threshold is observed in the Kr^{2+} spectrum, which was found to be a characteristic of such transitions. The threshold for discrete triplet ionization is observed in the inset of the Kr^{3+} spectrum, where it is just sufficiently separated from that of the 3d electrons. The spectrum for double O-shell ionization in Xe is shown in the inset of Fig. 4, together with the thresholds for formation of the $5s^25p^4$, $5s^15p^5$, and $5s^05p^6$ states. A few values obtained by Cairns et al. [18] in a photo-ionization experiment are also inserted in the figure. Their results are in excellent agreement with ours. However, the main conclusions from our coincidence measurements of the small angle inelastically scattered electrons in Kr and Xe and the ions formed are that we were able to demonstrate the presence of a minimum followed by a maximum in the contribution of the 4p–εd transitions in Kr and 5p–εd transitions in Xe. These minima and maxima were obscured in the photo-absorption measurements [20] by the rapidly rising contributions of 3d and 4d transitions in Kr and Xe, respectively. Furthermore, the results showed the existence of strong direct interaction between electrons in the outer and the inner shells, as opposed to a "shake off"-type interaction in Ar [15]. This gives evidence of the importance of the correlation between these shells of Kr and Xe, which is not considered in most of the calculations and is at least partially responsible for the discrepancies that exist between the experimental results of the oscillator strengths and those predicted by theory [21,22]. The electron–ion coincidence technique was also applied to study the K shell excitation of nitrogen and carbon monoxide

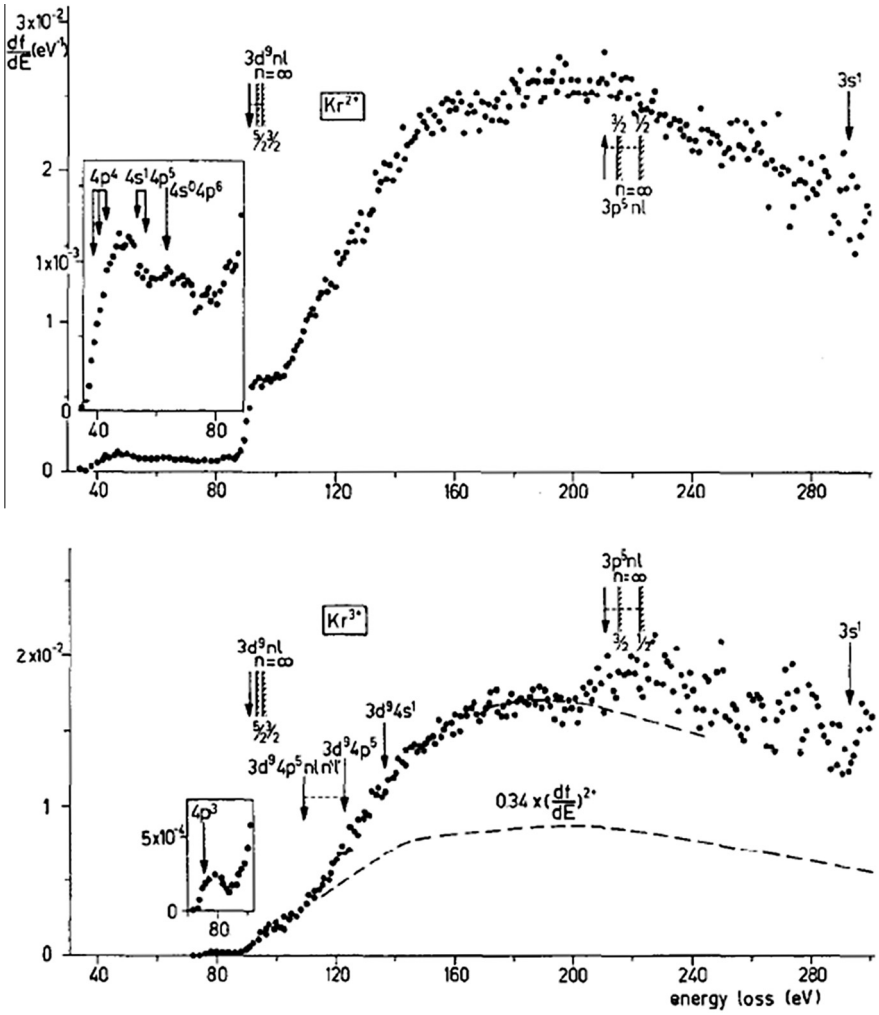

Fig. 3 Oscillator-strength spectra of Kr^{2+} and Kr^{3+}. The inset of the upper figure shows the direct ejection of two N electrons below the $3d^9$ threshold in the Kr^{2+} spectrum. The inset of the lower figure shows the threshold for discrete triple ionization in the Kr^{3+} spectrum.

by electron impact [23]. The study of the ionization of N_2 and CO by 10 keV electrons as a function of the energy loss was done by El-Sherbini and van der Wiel for the valence electrons [24] as well as for inner-shell electrons [25].

Our results on electron–atom ionization were the first of its type and corresponded well with those of photo-ionization by real and big synchrotron devices, but our apparatus was much faster and easier to operate. Our device was a sort of model synchrotron and in fact was considered to be **the first table-top synchrotron**.

Ion–atom collisions

Collision processes between fast heavy atoms and ions can be simply described by the interactions between relatively fast protons and alpha particles with neutral atoms. Besides the normal excitations and ionizations which are analogous to what happens in electron–atom collisions, an extra phenomenon occurs, named charge exchange. The best way to describe both types of phenomena is in treating the three particles involved, viz the point charge projectile, the target atom, and the electron with one Hamiltonian. It is one closed system in which kinetic energy of the projectile is transferred into electronic excitation energy. The impact parameter treatment has proven very useful, see Bates [26]. It gave a semiclassical description of the collision process, with the external motions classically and the internal motions quantum mechanically. Due to the heavy mass of the proton or alpha particle, the kinetic energy of the projectile is much bigger than the electronic excitations concerned. Therefore, the trajectory of the projectile is considered rectilinear during the whole collision event. The projectile keeps constant velocity, approximately. The impact parameter ρ is defined as the distance between the trajectory and the target nucleus. The cross-section σ for transition of the electronic system from state i to state f is given by

$$\sigma_{if}(E) = 2\pi \int_0^\infty \rho P(\rho) d\rho \tag{5}$$

where E is the kinetic energy of the projectile in the center of mass system, and

$$P(\rho) = |a_{if}(\rho, t = \infty)|^2 \tag{6}$$

with

$$i\frac{d}{dt}a_{if}(\vec{R}, t) = \sum_k a_{ik}(\vec{R}, t) V_{fk}(\vec{R}) \exp(-i\Delta E_{kf} t) \tag{7}$$

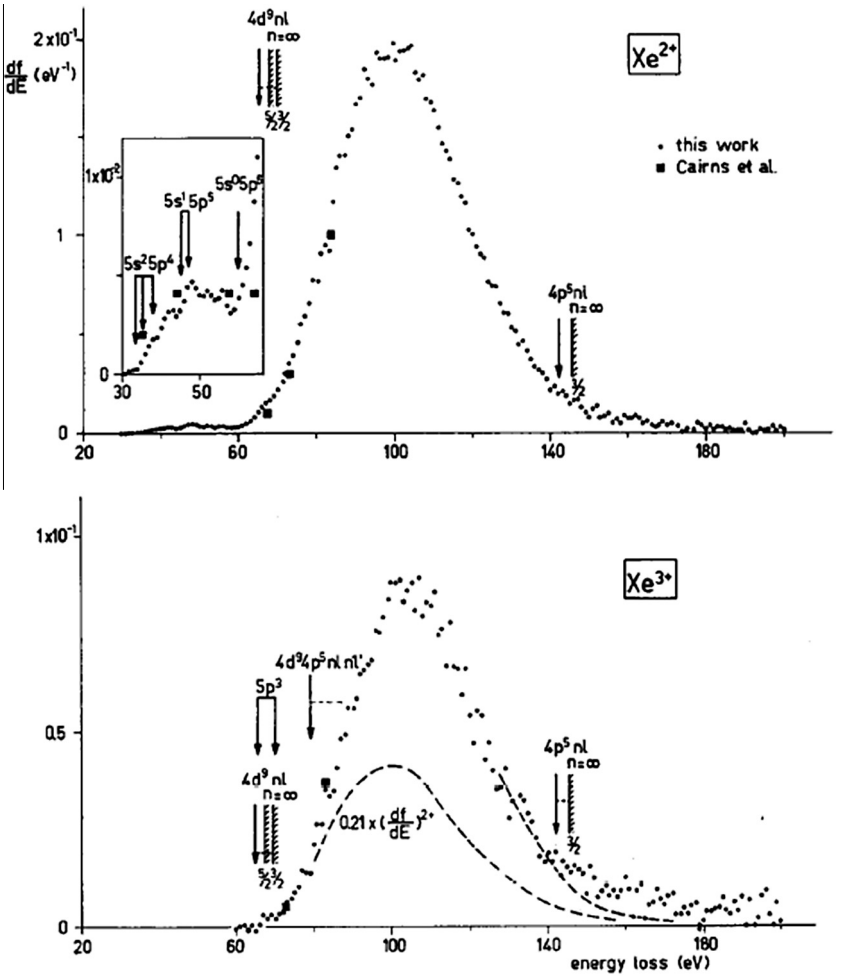

Fig. 4 Oscillator-strength spectra of Xe^{2+} and Xe^{3+}. The spectrum for double O-shell ionization is shown in the inset of the figure together with the thresholds for formation of the $5s^25p^4$, $5s^15p^5$ and $5s^05p^6$ states. Our data are plotted together with a few values obtained by Cairns et al. [18], from a photo-ionization experiment.

$$\Delta E_{kf} = E_k - E_f \tag{8}$$

$\vec{R}$ is the distance between both nuclei; $V_{fk}(\vec{R})$ is the matrix element of the potential field of target particle scaled by $\frac{2m}{\hbar^2}$ between the target eigen states f and k; E_k and E_f are eigen energies of target particle; and a_{ik} is the amplitude of the target eigen functions. For kinetic energies E far above the threshold, we can apply the Dirac condition, which assumes that the most dominant transition is from the initial to the final state i.e.

$$a_{ik} = \delta_{kf} a_{ik} \tag{9}$$

This leads to the integral equation

$$i a_{if}(\vec{R}, t) = \int_{-\infty}^{t} a_{if}(\vec{R}, \tau) V_{if}(\vec{R}) \exp(-i\Delta E_{if}\tau) d\tau \tag{10}$$

In the first order Born approximation, we obtain

$$i a_{if}(\rho, t = \infty) = \int_{-\infty}^{+\infty} V_{fi}(\vec{R}) \exp(-i\Delta E_{if} t) dt \tag{11}$$

see Merzbacher [27]. Replacing t by $\frac{z}{u}$, where u is the velocity, one gets

$$i a_{if}(\rho, t = \infty) = \frac{1}{u} \int_{-\infty}^{+\infty} V_{fi}(\vec{R}) \exp\left(-i\Delta E_{if} \frac{z}{u}\right) dz \tag{12}$$

From this relation, the dependence of $P(\rho)$ on u can be deduced. Therefore, it will depend on

$$\frac{a\Delta E_{if}}{u} \text{(in atomic units)} \tag{13}$$

One measures the effective interaction length "a" along the trajectory z, if the projectile passes by the target particle. This is the Massey Criterion. For large values of u, we see

$$\frac{a\Delta E_{if}}{hu} < 2\pi \tag{14}$$

which means that

$$P(\rho) \sim |a_{if}|2 \sim \frac{1}{u^2} \sim \frac{1}{E} \tag{15}$$

Decreasing speed coming from large values of u, one expects a maximum in $P(\rho)$ if $(a\Delta E_{if}/u \approx 2\pi)$, following the oscillatory behavior of $\exp(-i\Delta E_{if} z/u)$ as a function of u. This type of behavior has been studied by Hasted [28,29] who measured total cross-sections for exchange between various kinds of ions and neutral targets. Differential cross-sections, not only velocity dependent but also as a function of the scattering angle, have been measured by Morgan and Everhart [30] and by Kessel and Everhart [31].

Advances in this field were made by measuring electron capture by multiply charged ions. It attracted attention of many physicists in various fields of physics such as astrophysics, plasma physics, controlled thermonuclear fusion research, and X-ray laser production. When multiply charged ions collide with neutral particles (at low to intermediate impact velocities $u \leqslant 1$ au), capture reactions populating excited states in the projectile are very probable, see, for instance, Niehaus and Ruf [32] and Winter et al. [33]. For single electron capture, these reactions may lead to population inversion and are of importance in several schemes for the production of XUV and soft X-ray lasers. However, in these collisions, non-radiative (i.e. auto-ionizing) processes can be important, and competition with radiative processes occurs. Measurements of these non-radiative processes by Winter et al. [34] showed that the corresponding total cross-sections for the production of slow electrons were large and strongly charge state dependent. These results were interpreted by them to be the result of capture ionization, i.e., an Auger ionization in the short-lived quasi-molecule.

Let X^{z+} is the multiply charged ion and Y is the target atom, then the reactions can be followed by radiative emission

$$X^{z+} + Y \rightarrow X^{(z-1)+*} + Y^{+} \rightarrow X^{(z-1)+} + Y^{+} + h\nu$$

or by electron emission through one of the following channels

$$X^{z+} + Y \rightarrow X^{(z-1)+} + Y^{2+} + e \quad \text{(a)}$$

Auger ionization of the quasi-molecule formed during collision,

$$X^{z+} + Y \rightarrow X^{(z-1)+*} + Y+ \rightarrow X^{(z-1)+} + Y^{2} + +e \quad \text{(b)}$$

Penning ionization after single electron capture,

$$X^{z+} + Y \rightarrow X^{(z-2)+**} + Y^{2+} \rightarrow X^{(z-1)+} + Y^{2+} + e \quad \text{(c)}$$

double electron capture into autoionizing states of the projectile,

$$X^{z+} + Y \rightarrow X^{(z-1)+*} + Y^{+} \rightarrow X^{(z-2)+**} + Y^{2+} \quad \text{(d)}$$

$$\rightarrow X^{(z-1)+} + Y^{2+} + e \quad \text{(e)}$$

electron capture followed by electron promotion [35] into auto-ionizing states of the projectile.

The measurements of Winter et al. [34] yielded only total cross-sections for Ne^{z+} (z = 1–4) and Ar^{z+} (z = 1–8) colliding at energies 100 keV and 200 keV, respectively, with noble gas atoms. However, data on the energy spectrum of the electrons are still needed to investigate these phenomena in more detail. Woerlee et al. [36] have extended the work by measuring energy spectra of electrons produced in collisions of multiply charged neon ions with noble gas atoms. Fig. 5 shows the experimental results for 100 keV Ne^{1-4+} on Ar. The spectrum consists of a continuous background on which peaks are superimposed. The spectra for Ne^{1+} and Ne^{2+} are almost identical, but large changes are seen when the projectile charge state is increased from 2+ to 3+ and 3+ to 4+. The largest changes are an increase in the continuum below ±20 eV, and an increasing number of peaks superimposed on the continua. The increase in the continuum below 20 eV is the result of capture ionization in the short-lived quasi-molecule [37]. The bars in Fig. 5 indicate the positions of calculated transition energies corrected for a Doppler shift of −2.7 eV. The peaks observed in 100 keV $Ne^{3+,4+}$ on Ar shift to lower energies when the projectile energy is increased. This shift is equal to the kinematical shift, which would be expected, when the corresponding electrons are emitted by the projectile. Therefore, we concluded that the peaks originate from auto-ionizing states in the projectile, which decay after the collision has taken place. Since no photoabsorption data exist on the auto-ionizing states of multiply charged neon ions, we tried to calculate energy levels of doubly excited neon ions with a single configuration HF method. In order to determine the energies of the various levels, we included the electrostatic energy splitting due to the core electrons, see El-Sherbini and Farrag [38]. The energy splitting caused by the excited electrons is small and was not taken into account. We found that for Ne^{4+}–Ar, the peaks occur in the region for the calculated peak energies of Ne^{1+**}, Ne^{2+**}, and Ne^{3+**}, but Ne^{2+**} seems to cover most of the data. For Ne^{3+}–Ar, calculated energies of Ne^{1+**} and Ne^{2+**} appear in the region of the observed peaks.

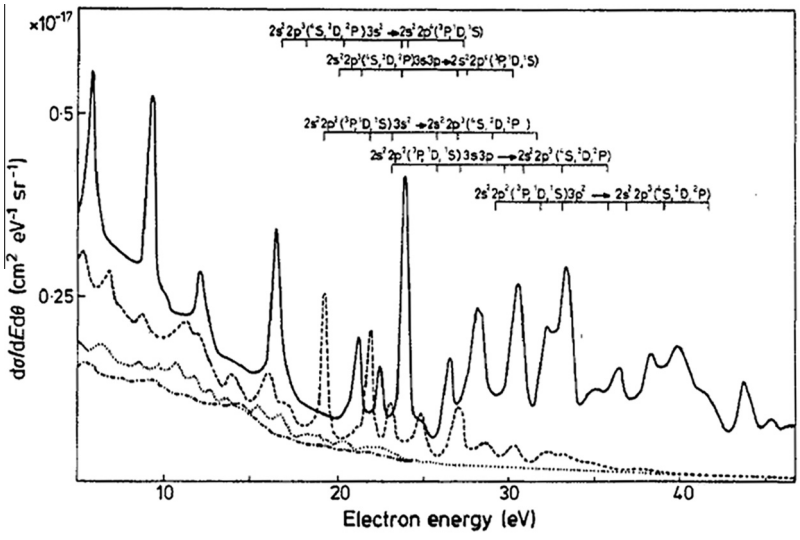

Fig. 5 Electron spectra for 100 keV Ne^{n+} on Ar ($\vartheta = 90°$), - - - - - - $n = 1$; ..... $n = 2$; – – – – – $n = 3$; ——— $n = 4$. The bars in the figure indicate the positions of calculated transition energies corrected for a Doppler shift of −2.7 eV.

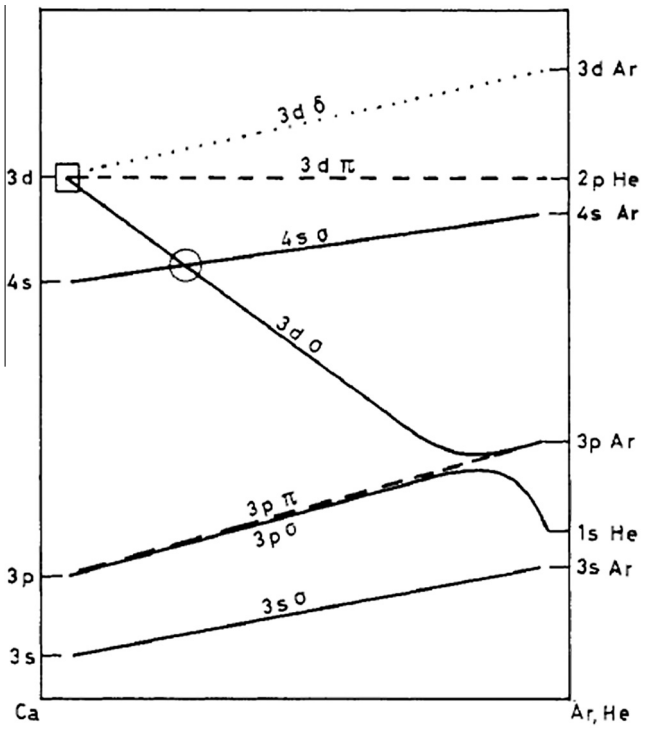

Fig. 6 Diabatic MO correlation diagram for Ar–He system. The radial coupling occurs at the 3dσ–4sσ crossing and the rotational coupling occurs at the 3dσ–3dπ–3dδ crossing.

Further developments in this field were done by El-Sherbini et al. [39], where they measured target dependence of excitation resulting from electron capture in collisions of 200 keV Ar^{6+} ions with noble gases. The study shows strongly rising total capture excitation cross-sections and shifts in the post-collision projectile excited-state distributions to higher n levels with the increase in the target atomic number. Energy dependence of excitation and ionization resulting from electron capture in Ar^{6+}–H_2 collision in the range of ion projectile energies 200–1200 keV was measured by El-Sherbini et al. [40]. These studies indicate that single electron charge transfer into excited states of the product ion is the most important inelastic process. Photon emission between 20 and 250 nm and slow electron and ion production cross-sections have been measured. The capture occurred mainly into $n = 4$ levels with the excitation of the higher angular momentum states dominating over most of the projectile energy range. The capture ionization cross-section is appreciable, amounting to 30–40% of the total excitation cross-section. These results are extremely valuable for the developments of controlled thermonuclear fusion reactors (see El-Sherbini [41]). To obtain more information about the coupling mechanisms, which gives rise to capture into excited states in ion–atom collisions at intermediate energies ($u \sim 0.5$ au), El-Sherbini and de Heer [42] measured photon emission in the spectral region between 60 and 100 nm in the collision of Ar^{q+} ($q = 1$, 2, and 3) with He and Ne at impact energies between 15 and 400 keV. The experimental results were explained qualitatively by considering the MO correlation diagram (Fig. 6). The emission cross-section for the collision of Ar^{q+} with He is shown in Fig. 7. It was often found that the cross-section for excitation decreases with the increase in the number of intermediate transitions required in order to reach the excited state. When there is a mechanism involving radial coupling leading from initial to final states, then it was found that the measured emission cross-section decreases with energy, where as mechanisms involving rotational coupling lead to cross-sections that increase with increasing energy up to 200 keV or more. The results have been of particular importance in evaluating theoretical models and have provided a valuable check of the range of validity of existing theories.

Atomic structure calculations and X-ray lasers

In the field of atomic collisions, as we noticed in the previous sections, much attention was paid to the excitation of noble gas atoms. A systematic study of the excitation process

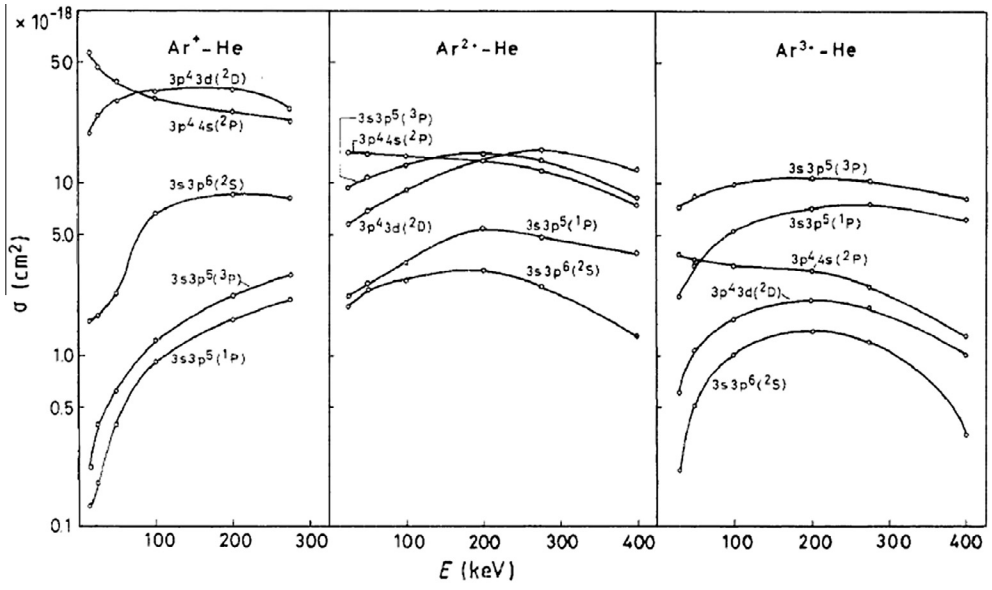

Fig. 7 Emission cross-section for Ar II ($3p^4 4s\ ^2P$), Ar II ($3p^4 3d\ ^2D$), Ar II ($3s3p^6\ ^2S$), and Ar III ($3s3p^5\ ^3P,^1P$) states plotted against projectile energy in Ar^{q+}–He collisions.

requires the knowledge of accurate dipole transition probabilities for spontaneous emission between the various configurations of the ions. Laser physics and astrophysics are other branches, which have stimulated more accurate atomic line strengths and transition probabilities calculations. Garstang [43,44] performed the first intermediate coupling calculations for Ne II. On this basis, Wiese et al. [45] composed their data compilations. However, the previously tabulated line strengths were in need of revision. In his work, Luyken [46,47] performed new calculations of line strengths and transition probabilities for Ne II and Ar II where specific configuration interactions were investigated and some effective operators were included. The results showed that the agreement with the experimental data was improved as compared with the earlier calculations. El-Sherbini [48–50] has extended the work of Luyken to the calculation of transition probabilities and radiative lifetimes for Kr II and Xe II. He used "exact" intermediate coupling wave functions to describe the various states [48] :

$$\Psi(J,M)=\sum \alpha_i|p^4 L_i^c S_i^c;\quad l_r\frac{1}{2};\quad L_i S_i JM> \tag{16}$$

where α_i is the expansion coefficient, J is the total angular momentum, M is the magnetic quantum number, L_i^c and S_i^c are the total orbital and spin angular momentum of the core electrons, l_r is the orbital angular momentum of the running electron, and L_i and S_i are the orbital and spin angular momentum of the pure L–S bases states on which the "exact" $\Psi(J,M)$ is expanded. The transition probability between two states with summation indices i and j refer to the upper and lower level, respectively, is given by

$$A(J_u,J_l)=\frac{64\pi^2}{3h\lambda^3(2J_u+1)}S(J_u,J_l) \tag{17}$$

where $S(J_u,J_l)$ is the line strength and J_u, J_l are the total angular momentum of the upper and lower states, respectively. The line strength is given by El-Sherbini [48]

$$\begin{aligned}S(J_u,J_l)=e^2\Bigg|\sum_{i,j}\alpha_i^*\alpha_j(-1)^{S_j+J_u+l_{ru}+L_j^c}\delta(S_i,S_j)\delta\left(L_i^c,L_j^c\right)\begin{Bmatrix}S_jL_jJ_l\\1J_uL_i\end{Bmatrix}\\ \begin{Bmatrix}L_j^c l_{rl}L_j\\1L_i l_{ru}\end{Bmatrix}\begin{pmatrix}l_{ru}1l_{rl}\\000\end{pmatrix}[(2J_u+1)(2J_l+1)(2L_i+1)\\ \left(2L_j+1\right)(2l_{ru}+1)(2l_{rl}+1)]^{1/2}\Bigg|^2\left(\int_0^\infty R_{l_{ru}}(r)rR_{l_{rl}}(r)dr\right)^2\end{aligned} \tag{18}$$

where J_u, J_l and l_{ru}, l_{rl} are, respectively, the total angular momentum of the states and the orbital angular momentum of the running electron in the upper and lower states. $R_{l_{ru}}(r)$ and $R_{l_{rl}}(r)$ are the one electron radial wavefunctions in the two different states.

The lifetime τ_u of the upper state is given by El-Sherbini [49]

$$\tau_u=\frac{1}{\sum_l A(J_u,J_l)} \tag{19}$$

The parametric potential method was used to calculate the radial part of the wave function [51], while the method of least squares fit of energy levels [52] was applied in obtaining the angular part of the wave function. The results obtained in intermediate coupling showed a much better agreement with the experimental data than those using pure LS-coupling wave functions. Further improvements in the atomic structure calculations of Kr II were obtained by El-Sherbini and Farrag [38] when including configuration interaction effects. The results showed that the $4s^24p^4(^1D)4d\ ^2S_{1/2}$ level is strongly perturbed through interaction with the $4s4p^6\ ^2S_{1/2}$ level, in agreement with the earlier predictions from the Kr II analysis. Theoretical investigations of the $5s^25p^45d + 5s^25p^46s + 5s5p^{6+}$ level structure in Xe II were performed by El-Sherbini and Zaki [53]. Taking into account, configuration-interaction effects in the calculations showed that some observed energy levels of the $5p^45d$ configuration were not correctly designated. A strong interaction between the $5p^45d$ and $5s5p^6$ configurations was also reported. Moreover, the calculated energies of the 6s and 5d levels were improved considerably by introducing configuration interactions into the calculations. The presence of strong configuration interaction between the $4s4p^6$, $4p^44d$, and $4p^45s$ configurations in singly ionized krypton [38] makes it difficult to perform accurate calculations for the energies, pumping rates, and lifetimes of levels in these configurations. Therefore, it was important to improve upon the previous calculations, see El-Sherbini [54,55], on the low lying $4p^44d$ and $4p^45s$ laser levels in this ion. Therefore, multi-configuration Hartree–Fock (MCHF) calculation in order to determine the lifetimes of these laser levels was done by El-Sherbini [56]. The results show that some of these levels are metastable. They also suggest a two-step excitation from the ground state of the ion to the $4p^45p$ level involving some intermediate metastable states as a possible laser excitation mechanism.

Further developments in the field of atomic structure calculations were done by the studies of excitation of electrons in atomic isoelectronic sequences [57–59]. These studies are essential not only for better understanding of atomic structure and ionizing phenomena, but also they provide new laser lines which could be extended into the X-ray spectral region [60,61]. This in turn will help in the development of X-ray laser devices. Once X-ray lasers become reliable, efficient, and economical, they will have several important applications. First and foremost, their short wave lengths, coherence, and extreme brightness should allow the exploration of living structures much smaller than one can see with optical methods. They will also have important applications in high resolution atomic spectroscopy, diagnostics of high density plasmas, radiation chemistry, photolithography, metallurgy, crystallography, medical radiology, and holographic imaging. Shortly after the demonstration of the first soft X-ray amplification in neon-isoelectronic selenium by Mathews et al. [62], extensive work was done both theoretically and experimentally on other systems [63,64]. Progress toward the development of soft X-ray lasers with several plasma-ion media of different isoelectronic sequences was achieved at many laboratories [65,66]. A soft X-ray laser transitions in the Be-isoelectronic sequence were proposed by Krishnan and Trebes [67]. They suggested that intense line radiation from plasmas of Mn VI, P IV, Al V, Al V III, Al IX, and Al XI may be used to selectively pump population inversions in plasmas of Be-like C III, N IV, F VI, and Ne VII and Na VIII. Lasing in the soft X-ray region is then possible on 4p–3d and 4f–3d (singlet and triplet) transitions. Short wave length laser calculations in the beryllium sequence were done by Feldman et al. [68]. They calculated gain at a number of different temperatures and electron densities for the 3p–3s laser transition in the highly charged ions of Be-sequence. Al-Rabban [69] has extended both the work of Krishnan and Trebes [67] and Feldman et al. [68], to the higher members of the Be-isoelectronic sequence and to more transition states (which are promising for X-ray laser emission). She

carried out an ab initio multi-configuration Hartree–Fock calculations of energy levels, atomic oscillator strengths, and radiative lifetimes for singly and doubly excited states in Be I and Be-like ions. Configuration interaction effects between the various configurations were included using the computer program code CIV3 described by Hibbert [70]. In this code, the N-electron energies and eigenfunctions are obtained by diagonalizing the Hamiltonian matrix, which may have quite large dimensions. The choice for the spatial (radial) part of the single particle wave functions is based on expansions in Slater-type orbitals [71]:

$$P_{nl}(r) = \sum_{j=1}^{k} C_{jnl} r^{I_{jnl}} \exp(-\xi_{jnl} r) \tag{20}$$

The coefficients in the expansion C_{jnl}, I_{jnl} as well as ξ_{jnl} in the exponents are treated as variational parameters.

Investigations of the possibilities of obtaining population inversion and laser emission could be achieved by calculating the level population of the excited states. These calculations were done by the group of atomic physics at the Physics Department of the Faculty of Science – Cairo University, solving the coupled rate equations [72]

$$N_j \left[\sum_{i\langle j} A_{ji} + N_e \left(\sum_{i\langle j} C^d_{ji} + \sum_{i\rangle j} C^e_{ji} \right) \right] = N_e \left(\sum_{i\langle j} N_i C^e_{ij} + \sum_{i\rangle j} N_i C^d_{ij} \right) + \sum_{i\rangle j} N_i A_{ij} \tag{21}$$

where N_j is the population density of level j, A_{ji} is the spontaneous decay rate from level j to level i, C^e_{ji} is the electron collisional excitation rate coefficient, C^d_{ji} is the electron collisional de-excitation rate coefficient, and N_e is the plasma electron density. The gain coefficient (α) for Doppler broadening of the various transitions is given by Elton [73] :

$$\alpha = \frac{\lambda^2_{lu}}{8\pi} \left(\frac{M}{2\pi k T_i} \right)^{1/2} A_{ul} N_u F \tag{22}$$

where M is the ion mass, λ_{lu} is the transition wave length in cm, T_i is the ion temperature in K, u and l represent the upper and lower transition levels, respectively, N_u is the population of the upper level, and F is the gain factor.

Vriens and Smeets [74] gave empirical formulas for the calculation of rate coefficient in hydrogen atom. Their work was

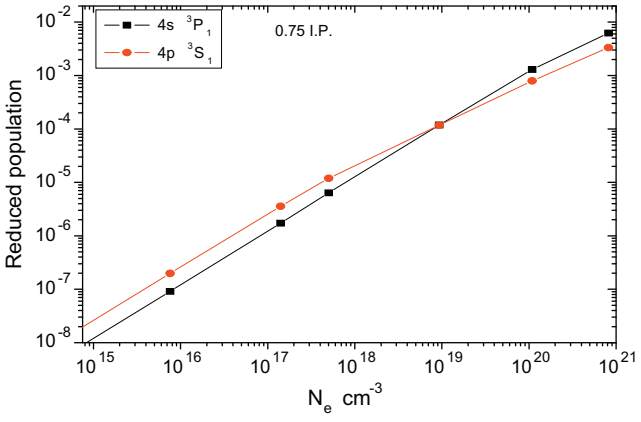

Fig. 8 Reduced fractional population for selected levels of Ni^{14+} ions at electron temperature 3/4 the ionization potential.

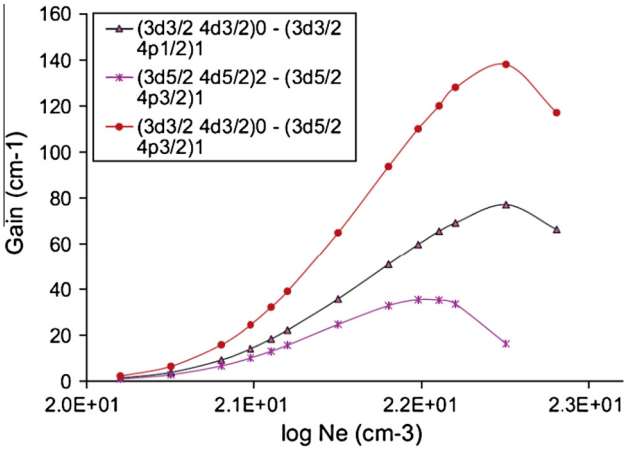

Fig. 9 Gain coefficient of laser transitions against electron density at temperature 2 keV in E_u^{35+} ions.

extended by Allam [75] to be valid for atoms with one electron outside a closed shell and also for two-electron atoms (ions). Allam [75] adopted the method of Palumb and Elton [76] for modeling plasmas of helium-like and carbon-like ions, and he has developed a computer program (CRMOC) in order to calculate excitation and de-excitation rate coefficients for two-electron system. In his program which was developed for collisional radiative model calculations, the principal quantum numbers of the excited states were replaced by effective quantum numbers. Using the above theoretical schemes, the atomic physics group was able to extensively investigate the possibility of X-ray laser emission in several isoelectronic systems, see for example Figs. 8 and 9. The studies include helium isoelectronic sequence [77], beryllium isoelectronic sequence [69,78], boron isoelectronic sequence [79–81], carbon isoelectronic sequence [82], sodium isoelectronic sequence [83–85], magnesium isoelectronic sequence [86–88], aluminum isoelectronic sequence [89], silicon isoelectronic sequence [90–92], sulfur isoelectronic sequence [93], potassium isoelectronic sequence [94], scandium isoelectronic sequence [95], and nickel isoelectronic sequence [96]. Most of the heavy members of the isoelectronic sequences studied radiate in the XUV and Soft X-Ray spectral regions (λ between 50 and 1000 Å). The reported stimulated emission transitions in these ions indicate that some of the transitions are promising and could lead to progress toward the development of XUV and Soft X-Ray lasers.

Laser-induced breakdown spectroscopy (LIBS)

Laser-induced breakdown spectroscopy is a form of optical (atomic) emission spectroscopy [97]. It is a technique based on utilizing light emitted from plasma generated via interaction of a high power lasers with matter (solids, liquids or gases). Assuming that light emitted is sufficiently influenced by the characteristic parameters of the plasma, the atomic spectroscopic analysis of this light shows considerable information about the elemental structure and the basic physical processes in plasmas. There is a growing interest in LIBS, particularly in the last 20 years because of its applications in the laboratory and in industry, art, environment, medicine, and forensic sciences [98–100]. Most commonly, LIBS has been applied to sensitive elemental analysis of solids, conductors

and non-conductors, as well as liquid and gaseous samples [101]. It has many practical advantages over more conventional elemental analysis techniques. LIBS has been utilized to analyze thin metal films [102], and it has found more and more applications in monitoring of industrial processes [98], characterization of jewellery products [103], soil studies [104], pulsed laser thin film deposition [105], quality control of pharmaceutical products [100], cleaning [106], and in situ planetary exploration [107].

An enhancement of the LIBS sensitivity was achieved by introducing the double pulse technique [108]. The double pulse (DP)-LIBS configuration, which makes use of two laser pulses separated by a suitable temporal delay instead of a single pulse for inducing the plasma, was reported to give a substantial enhancement of the signal to noise ratio with respect to single pulse (SP)-LIBS configuration with a corresponding improvement of the limits of detections [109]. The double pulse laser ablation (DPLA) approach in relation to the spectral analysis was first reported by Piepmeier and Malmstadt [110]. However, the first systematic investigation of (DPLA) was reported by Sattmann et al. [111]. They performed a quantitative microchemical analysis of low-alloy steel with single and double laser pulses, where they found that the analytical performance was considerably improved by the double pulse technique. The great contribution to the development of (DPLA) for practical analysis was made by Petukh et al. [112]. They compared radiation of plasma flares produced on exposure of metals to laser radiation in a monopulse generation mode in the case of single and double pulses with change in air pressure. They observed in the case of double pulses increases in the duration and the intensity of the radiation of the spectral lines. For elucidation of the double pulse laser ablation (DPLA) mechanisms, see, for instance, St-Onge et al. [113] and Noll [114]. DP-LIBS technique was also applied for the fabrication of nanosize particles. Tarasenko et al. [115] studied and analyzed the capabilities of laser ablation in liquids for fabrication metallic and composite nanoparticles. The technique offers the better controle over the particle formation process. They found that the mean size of the nanoparticles and their stability could be controlled by proper selection of the parameters of laser ablation such as temporal delays between pulses, laser fluence, and the sort of liquid used. Therefore, the optimal conditions favoring the formation of nanoparticles with a desired structure could be reached.

Parallel to the work on atomic structure calculations by our atomic physics group at the physics department, the group was also involved in the study of the physical parameters of plasmas generated by high power laser irradiation of solid targets (plasma diagnostics), applying the (LIBS) technique. The spectroscopic plasma diagnostics which is essentially based on the measurements of the optical radiation emitted from the plasma enables the group to obtain simultaneously a large amount of information about the plasma without disturbing it. Spectral fingerprints of optical plasma emission provide information about the physical and chemical processes that occur in the plasma. The spectra can contain individual spectral lines, band, or continuum radiation. Plasma emits line radiations resulting from bound–bound electronic transitions and continuum radiations resulting from free-bound and free–free electronic transitions. However, utility of spectroscopic diagnostics depends upon the knowledge about radiative behavior of atomic and molecular species and type of equilibrium attained in the plasma. It is assumed that the plasma in our laboratory (laboratory of lasers and new materials at the physics department) is in local thermodynamic equilibrium (LTE). In local thermodynamic equilibrium, all the species in the plasma, i.e., electrons, ions, and neutrals are in thermodynamic equilibrium except the radiation. This condition generally is observed to be valid in a collision dominated plasma such as high-pressure arc plasma produced in plasma torches. Small size of such plasmas allows radiation to escape to the surroundings. In (LTE) plasmas, the number of electronic transitions due to collisions between the first excited states and the fundamental level is 10 times larger than the number of transitions due to spontaneous emission. Collisions are mainly responsible for excitation and de-excitation, ionization, and recombination. The two main parameters that characterized the state of the plasma are namely the plasma temperature and the electron density. Knowledge of the temperature leads to understand the plasma processes occurring such as vaporization, dissociation, ionization, and excitation. The optical emission spectroscopic (OES) method for the determination of the plasma temperature is based on the measurements of the intensity of the spectral lines. In optically thin plasma, the integrated intensity of an atomic emission line is related to excitation energy, population density of upper state and transition probability as given by

$$I_{ul} = \frac{1}{4\pi} A_{ul} n_u h\upsilon_{ul} L \ (\mathrm{W/m^2\text{-}ster}) \tag{23}$$

where I_{ul} is the line intensity of transition from upper level u to lower level l integrated over the plasma length L, A_{ul} is the spontaneous transition probability, n_u is the density of atom excited in the upper energy level u, and $h\upsilon_{ul}$ is the energy of each emitted quantum. The measurement of I_{ul} gives only the population of upper level u. When the thermal plasma is in (LTE), the density of atoms excited to the upper level is given by the Boltzmann distribution function:

$$n_u = \left(\frac{n_0}{Z_0}\right) g_u \exp\left(\frac{-E_u}{kT}\right) \tag{24}$$

where n_0 is the total density of atoms, g_u is the statistical weight of the upper state, E_u is the energy of upper state, k is Boltzmann constant, and Z_0 is the partition function defined by

$$Z_0 = \sum_u g_u \exp\left(\frac{-E_u}{kT}\right) \tag{25}$$

Substituting the value of n_u into Eq. (23), we get

$$I_{ul} = \frac{1}{4\pi} \frac{hcA_{ul}}{\lambda_{ul}} \frac{n_0 L}{Z_0} g_u \exp\left(\frac{-E_u}{kT}\right) \tag{26}$$

In case of the evaluation of absolute line intensity, one should know the initial composition, pressure and wave length of the emission line. The values of A_{ul}, g_{ul}, and E_u can be obtained from spectroscopic tables. However, one must also know the plasma length, and an absolute spectral radiance calibration must be performed using a standard source. For relative line intensities measurement of the same species and stage of ionization, one needs not to know the values of partition function, n_0, and plasma emitting length. The ratio of two emission lines I_1 and I_2 is given by

$$\frac{I_1}{I_2} = \frac{g_1 A_1 \lambda_2}{g_2 A_2 \lambda_1} \exp\left(\frac{E_2 - E_1}{kT}\right) \tag{27}$$

The terms in Eq. (26) can be arranged as

$$\frac{I_{ul}\lambda_{ul}}{g_u A_{ul}} = \frac{hcn_0 L}{4\pi Z_0}\exp\left(\frac{-E_u}{kT}\right) \tag{28}$$

and therefore, we can write

$$\ln\left(\frac{I_{ul}\lambda_{ul}}{g_u A_{ul}}\right) = B - \frac{E_u}{kT} \tag{29}$$

This is an equation of straight line where $B = \ln(hcn_0 L/4\pi Z_0)$ is a constant. If $\ln(I_{ul}\lambda_{ul}/g_u A_{ul})$ values are plotted against E_u, the temperature is given by the reciprocal of the slope of the straight line. This is called the atomic Boltzmann plot method. The other key parameter in the diagnostics of plasma is the electron density. Determination of the electron density n_{ek} is based on the broadening of emission lines from the plasma. It is assumed that the Stark effect is the dominant broadening mechanism, in comparison with Doppler broadening and the other pressure broadening mechanisms, due to collisions with neutral atoms. The validity of this assumption was generally admitted in works on (LIBS) and is justified in various studies [116,117]. For the linear Stark effect (hydrogen and hydrogenic ions), the following equation is valid [116]

$$n_e = C(T, n_e)\Delta\lambda_s \tag{30}$$

where $\Delta\lambda_s$ is the full width at half maximum (FWHM) of the spectral line and $C(T, n_e)$ is a coefficient that is only a weak function of electron density and temperature. For elements other than hydrogen and hydrogen-like ions, the quadratic Stark effect acts on the total half width at half maximum (HWHM), due to collisions with electrons and ions, ω_{total} is approximately given by Griem [117]

$$\omega_{total} = [1 + 1.75A(1 - 0.75R)]\omega_s n_e / n_e^{ref} \tag{31}$$

where ω_{total} is the electron impact (half) width, A is the ion broadening parameter, ω_s is the Stark width, n_e^{ref} is a reference electron density, usually of the order of 10^{16} or 10^{17} cm^{-3}, and R is the ratio of the mean distance between ion and Debye radius. Eq. (31) is used in LIBS to determine the electron density from experimentally measured line widths of selected lines. For accurate measurements of the electron density, spectral lines as isolated as possible and emitted in optically thin conditions have to be selected. Stark broadening of isolated spectral lines of non-hydrogenic neutral atoms and ions is due mainly to electrons. As a consequence, the contribution of quasi-static ions was generally neglected, and hence, the Lorentzian FWHM can be approximated by

$$\omega_{total} = \omega_s(n_e / n_e^{ref}) \tag{32}$$

Our group at the laboratory of lasers and new materials at the physics department has studied emission spectra from laser-induced titanium plasma [118] and measured population density and temperature of argon metastable ($^1S_3$) state using tunable diode laser-absorption diagnostic technique [119]. An elemental analysis of some minerals using laser-induced breakdown spectroscopy (LIBS) was performed at the laboratory by El-Sergany et al. [120].

Self-absorption effect can distort the spectral line shape and therefore produces apparently an increase in the line width and a decrease in the line intensity, Griem [116]. It is originated mostly from cooler boundary layer of the plasma which contains much lower population density [117]. This effect will mislead investigators and can give in accurate results for the plasma parameters. Therefore, for the work on LIBS, one has to check the presence of self-absorption. Our group has evaluated self-absorption coefficient of Aluminum emission lines in laser-induced breakdown spectroscopy (LIBS) measurements, see El-Sherbini et al. [121]. Hydrogen lines, especially those of the Balmer series exhibit linear Stark effect, are the most strongly broadened lines, and they are easy to measure. Therefore, they are oftenly used to determine the electron density. Our group, El-Sherbini et al. [122], has measured the electron density in a laser produced plasma experiment using the Stark broadening of H_α-line at 656.27 nm. This line is produced from the interaction of a Q-switched Nd-Yag laser beam at the fundamental wave length of 1.06 μm with a plane solid aluminum target in a humid air Fig. 10. In this experiment, light emitted from the plasma plume is collected by a lens and optical fiber arrangement using an imaging spectrograph with ICCD camera, see Fig. 10. The wave length scale was calibrated with a low pressure Hg-lamp. The emitted light was collected in the wave length region from 200 to 1000 nm. The gain of the camera was kept fixed at a maximum level of 250. The measurement was confirmed by observing the spectra emitted at wave length regions from plasma at delay times from 30 to 50 μs which gave the same band width. Identification of the different spectral lines was carried out using a software spectrum analyzer (version 1.6). The agreement between the measured electron density from both the H_α-line and the Al II-line at 281.62 nm confirms the reliability of utilizing the H_α-line as an electron density standard reference line in LIBS experiments.

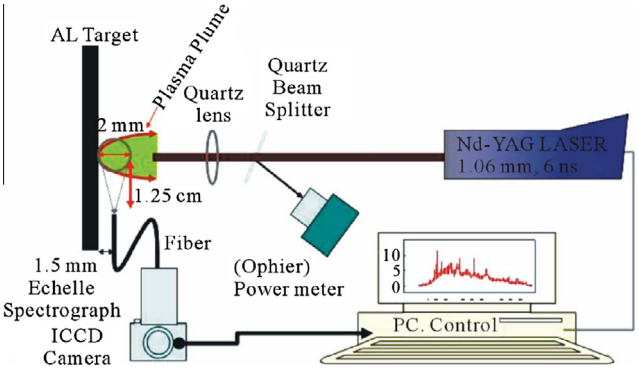

Fig. 10 Experimental set up.

Our group has also measured the Stark broadening of atomic emission lines in non-optically thin plasmas by of laser-induced breakdown spectroscopy, El-Sherbini et al. [123]. An assessment of LIBS diagnostics of plasma using the hydrogen H_α-line at different laser energies in air was performed by the group, El-Sherbini et al. [124]. Moreover, the atomic physics group has applied the diode laser atomic absorption spectroscopy (DLAAS) technique to assess the degree of optical opacity of plasma at the wave length of H_α-line, El-Sherbini et al. [125]. They found that the plasma associated with metallic targets is almost optically thin at the H_α-line over all fluencies and at delay times $\geqslant 1$ μs, but rather thick for hydrogen-rich targets (plastic and wood) over all delay times and fluencies.

Recent measurements of plasma electron temperature utilizing magnesium lines appeared in laser produced aluminum plasmas were done by the group, El-Sherbini et al. [126]. This work shows that the Mg I and Mg II lines appeared at the short

wave length region of the LIBS spectrum are good candidates for measuring the temperature of the plasma in LIBS experiments, but after correction against self-absorption. The spectrometric measurements of plasma parameters utilizing the target ambient gas O I and N I atomic lines show the reliability in the values of the electron density and the temperature of the plasma generated by the interaction of laser beam with solid targets, El-Sherbini et al. [127].

Advances in the LIBS measurements at our laboratory of lasers and new materials in the physics department at the faculty of science – Cairo University were achieved by studying the X-ray/particle emission from plasmas produced by laser irradiating nano-srtuctured targets, Hegazy et al. [128]. In this experiment, nano-copper structures evaporated onto copper bulk disks and nano-gold structures evaporated onto gold ones were used. An ion collector and X-ray semiconductor diode were used to study the ion and X-ray emission, respectively. A comparison of both studies in the case of nano-structured targets and bulk targets was performed at different laser fluencies (1×10^9–1×10^{12} W/cm^2) on the target. A 20% increase in the X-ray emission for nano-gold with respect to the bulk gold was observed; however, the X-ray emission in the nano-copper and copper was the same. At high laser intensities, the presence of non-linear processes in the preformed plasma may significantly increase the temperature of the fast electrons, and therefore mainly, the hard components of X-ray radiation at the fast ion emission are produced that does not happen in low energy nano-second experiments. Another progress was also recently achieved at our laboratory, by observing enhancements in LIBS signals from nano vs. bulk ZnO targets and nano-based targets, El-Sherbini et al. [129]. The study revealed that the signal enhancement cannot be attributed to the plasma temperature difference or the difference in the electron density. The signal enhancement depends only on the relative atomic concentration in the plasma created from the nano-based material with respect to the bulk-based plasma. This can be qualitatively explained in terms of the collisonal radiative modeling; for an electron density in the order of 10^{17} cm^{-3}, the collision processes are the dominant ones. Therefore, the enhanced emission of Zn I-lines from the nano-based target Fig. 11 could be attributed to the higher concentration of neutral atoms in the nano-based material plasma with respect to the corresponding bulk-based ZnO material.

The evolution of Al plasma generated by Nd-YAG laser radiation at the fundamental wave length was studied at our laboratory by Hegazy et al. [130]. The results showed that the plasma temperature and the electron density are strongly dependent on the time and on the laser energy. More recently, another study was done at our laboratory by the same authors on titanium targets [131]. They investigated the spectral-evolution of nano-second laser interaction with Ti target in air. In this study, time resolved optical emission spectroscopy (OES) has been successfully employed to investigate the evolution of plasma produced by IR- and visible-pulsed laser beams irradiating a titanium target in ambient air at atmospheric pressure. The characterization of the plasma-assisted pulsed laser ablation of the titanium target was discussed. The obtained temperature was in a good agreement with the one obtained from Ti II spectral lines previously suggested by Herman et al. [132]. Moreover, the Stark broadening method has been employed in the experiment for electron density measurements.

In conclusion, plasma diagnostic technique with LIBS is essential for accurate determination of plasma parameters such as temperature and electron density. It can give more

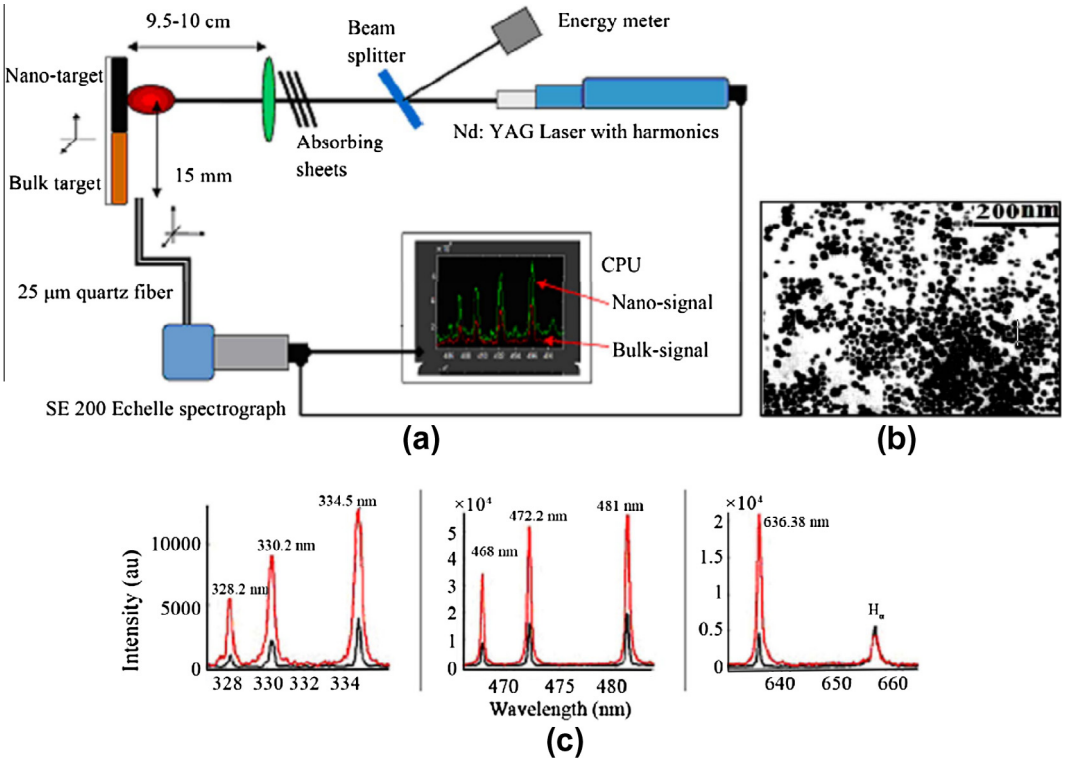

Fig. 11 (a) experimental setup; (b) TEM image of the ZnO-20 nm size; (c) enhanced emission of the Zn I – line from the nano-based target (red color) in comparison to that from the bulk-based material (black color).

information about the atomic processes and the dynamic nature of the plasma. This information plays a major role in astrophysics and in controlled thermonuclear fusion research.

Laser cooling and Bose–Einstein condensation

One of the research highlights in atomic physics in recent years is the study of laser cooling and Bose–Einstein condensation. As early as 1917, Einstein [133] had predicted that momentum is transferred in the absorption and emission of light, but it was not until the mid eighties that such optical momentum transfer was used to cool and trap neutral atoms [134,135]. By properly tuning laser light close to atomic transitions, atomic samples can be cooled to extremely low temperatures [136]. In 1985, National Bureau of standards group [137] cooled atoms in a thermal atomic beam in the range of 50–100 m K by irradiating them with a beam of counter-propagating against their motion. If the laser is tuned to the low frequency side of an atomic resonance, an atom moving against the direction of a laser beam will see the beam Doppler-shifted into resonance, while the beam co-propagating with the atom will be Doppler-shifted out of resonance. Thus, the atom will preferentially scatter photons from the beam opposing the direction of motion. A step further was cooling in three dimensions, and this was accomplished by creating three sets of counter-propagating beams along the x, y, and z axes. The idea was suggested by Hansch and Schawlow [138] and was demonstrated by Chu et al. [139] . Because the cooling force is viscous (linearly proportional to the velocity of atoms for low velocities), the laser beams that generate the drag force was named "optical molasses."

A substantial improvement in laser cooling was achieved with optical molasses (OM), where three intersecting orthogonal pairs of oppositely directed laser beams are used to severely restrict the movement of atoms in the intersection region. With this technique, atoms could be cooled to temperatures between 1 and 0.1 μK. The first cooling and trapping of neutral atoms (sodium atoms) was accomplished with optical molasses in combination with magneto-static fields Fig. 12, and the technique was named magneto-optical trapping MOT [140].

When atoms in a gas are cooled to extremely low temperatures, they will (under the appropriate condition) condensate into a single quantum mechanical state known as a Bose–Einstein condensate (BEC). This phenomenon was predicted

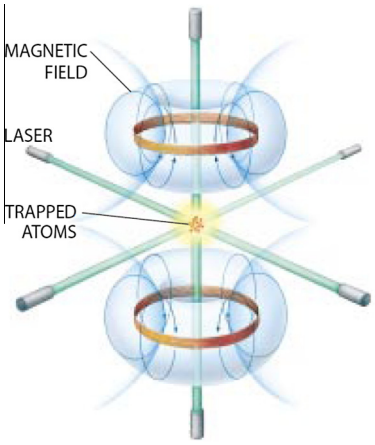

Fig. 12 The technique of magneto-optical trapping MOT, Scientific American (January 1998).

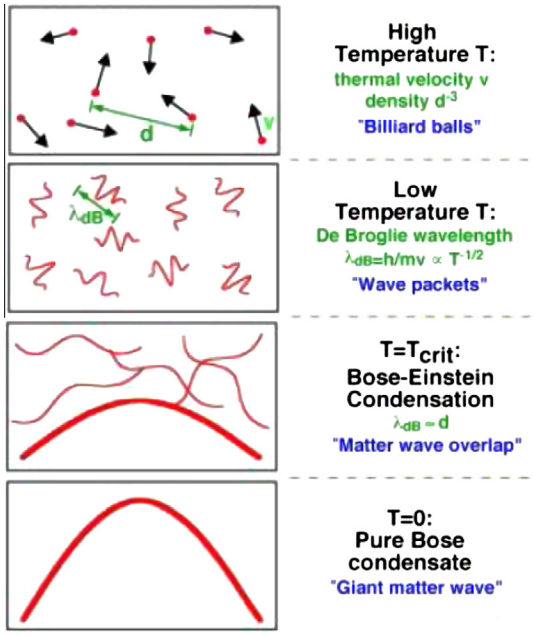

Fig. 13 A diagram showing the properties of particles in a gas at various temperatures, Ketterle [142].

by Nath Bose and Albert Einstein in 1925 when they pointed out that at low temperatures particles in a gas could all reside in the same quantum state. The Bose–Einstein condensation exhibits a new state of matter which occurs at extremely low temperatures when the de Broglie wave length of atoms becomes comparable to the average distance between them Fig. 13. The temperatures reached by laser cooling are impressively low, but they are not low enough to produce BEC in gases at the densities that are realizable experimentally. In the experiments performed to obtain BEC of alkali gases, evaporative cooling which was first suggested by Hess [141] was used after laser cooling. With this additional cooling, the temperature reached about 2 nK, which was sufficiently low to form BEC. The basic physical effect in evaporative cooling is that if particles escaping from a system have energy higher than the average energy of particles in the system, the remaining particles are cooled. If one makes a hole in the magneto-optical trap (MOT), only atoms with an energy at least equal to the energy of the trap at the hole will be able to escape. In practice, one can make such a hole by applying radio-frequency radiation that flips the spin state of an atom from a low-field seeking one to a high field seeking one, thereby expelling the atom from the trap [142]. In order to diagnose the dense and cold samples of trapped atoms, the time of flight (TOF) method is used [143]. The (TOF) method was capable of mapping out the velocity distribution for both hyperfine and ground states of dilute gases of alkali atoms along their path through the trap, see Fig. 14. The peculiar BEC gaseous state was created and diagnosed in the laboratory for the first time in 1995, by Carl Wieman, Cornell, and co-workers [144] at the JILA laboratory in Boulder and by Ketterle and co-workers [145] at the MIT, using the powerful laser cooling method together with evaporative cooling method. Nowadays, the phenomenon of BEC has become an increasingly active area of research both experimentally and theoretically. Research work on this form of matter is relevant to many different areas of physics – from atomic clocks and

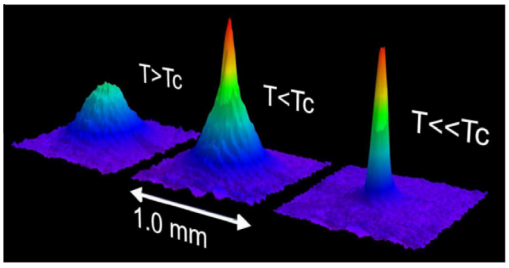

Fig. 14 The density profile of the condensate after time of flight expansion, giving emphasis to the velocity distribution, Ref. [144].

quantum computing to superfluidity, superconductivity, atom lasers, and quantum phase transition.

The pioneering work on BEC by Wieman, Cornell and Ketterle and others [144–146] was centered on atoms that were bosons, particles with integer spins. But atomic physicists have since extended their work to create Fermi gases from atoms that are fermions, particles with half odd integer spins. The advances came in 2003 by Deborah Jin and co-workers at the university of Colorado [147], who created a BEC of weakly bound molecules from ultra-cold Fermi gas of potassium-40 atoms. This new form of matter may help in a better understanding of superconductivity and could pave the way toward a superconductor that works at room temperature. Recently, research efforts in the field of BEC were directed toward storing ultra-cold bosonic and fermionic quantum gases in artificial periodic potentials of light, i.e., in optical lattices [148]. This has opened innovative manipulation and control possibilities, in many cases creating structures far beyond those currently achievable in typical condensed matter physics systems. Trapping ultra-cold quantum gases in optical lattices will open the door to a wide interdisciplinary field of physics ranging from non-linear dynamics to strongly correlated quantum phases and quantum information processing.

Around 2004, the group of atomic physics at the Physics Department of the Faculty of Science – Cairo University started theoretical work on BEC, and a brief review on the subject was given by El-Sherbini [149]. The group adopted in their studies the semiclassical approximation, i.e., the density of state (DOS) approach [150]. In this approach, the sum over the discrete spectrum for the thermodynamic quantities of the Bose–Einstein condensate was replaced by an integral weighted of a piecewise DOS. The latter was calculated via the technique of the high temperature expansion for the partition function [151]. This approximation has been widely used in variety of problems in statistical physics [152]. These studies showed that the resulting thermodynamic parameters depend crucially on the choice and construction of the DOS [153].

A generalization of the semiclassical approximation was suggested by Hassan and El-Badry [154], allowing for an essential extension of its region of applicability. The parameterized DOS has considered the effects of finite size, anisotropic of the harmonic potential, and the positive chemical potential; all of them simultaneously. The latter effect is similar to the effect of repulsive interaction provided by the mean field theory approach [155]. The outcome results provide a solid theoretical formulation for the existing experiments [155]. The generalized semiclassical approximation was also applied by Hassan and El-Badry [156] in the study of thermodynamic properties of quasi-equilibrium magnons in crystalline bulk materials and thin films and by Hassan [157] in the calculations of effective area and expansion energy of trapped Bose gas in a combined magnetic-optical potential. Hassan et al. [158] were able to calculate the critical temperature of a Bose–Einstein condensate in a 3D non-cubic optical lattice. Moreover, Hassan et al. [159] have studied recently the thermodynamic properties of condensed 39 K Bose gas in a harmonic trap. In particular the critical atoms number and its corresponding temperature are predicted via the graphical representation [160]. A step further in the advancement of research on BEC was carried out by the group, where they determined the thermodynamic properties of rotating Bose gas in a harmonic trap [161].

Nowadays, the work on fast rotating gases in Bose Einstein condensates which was initiated by the group of Dalibard at the Ecole Normale Superieure (ENS) laboratory in Paris [162] was recently under investigation by our group. Usually, the effective trapping potential V_{eff} for fast rotation regime is approximated by harmonic plus weak quartic potential [163]:

$$V_{eff} = \frac{m}{2}[\omega_z^2 z^2 + \omega_\perp^2 r_\perp^2] + \frac{1}{4}xr^4 - \frac{m}{2}\Omega^2 r_\perp^2 \tag{33}$$

where m is the mass of the atom and $r^2 = x^2 + y^2$ is the perpendicular radius to the rotation axis z. The parameter x classifies the strength of the quartic term and, moreover, plays an important role in exploring the fast rotation regime. The parameter κ must be greater than zero; otherwise, the effective potential felt by the atom V_{eff} would tend to $-\infty$ for $r \to \pm\infty$.

In a recent paper by the group, El-Sherbini et al. [164], a modified semiclassical approximation is provided to study the effects of finite size, the positive chemical potential, and anisotropy of the trap, on the thermodynamical properties of a rotating gas in a harmonic plus quartic trap. Fig. 15 presents the characteristic dependence of the condensate fraction N_0/N on the reduced temperature T/T_0 and the rotation rate α. It shows the monotonically decreasing nature of the condensate fraction due to the increase in the reduced temperature everywhere. This decrease is minor in the slow rotation range and rapid in the fast rotation range monotonically in agreement with the experimental observations and the numerical calculation [165]. Our results also provide a correction due to the finite size and positive chemical potential effects (interaction effect) for the results of Kling and Pelster [165]. Both of them show a significant quenching of the condensate fraction and a shift of the critical temperature toward the lower values.

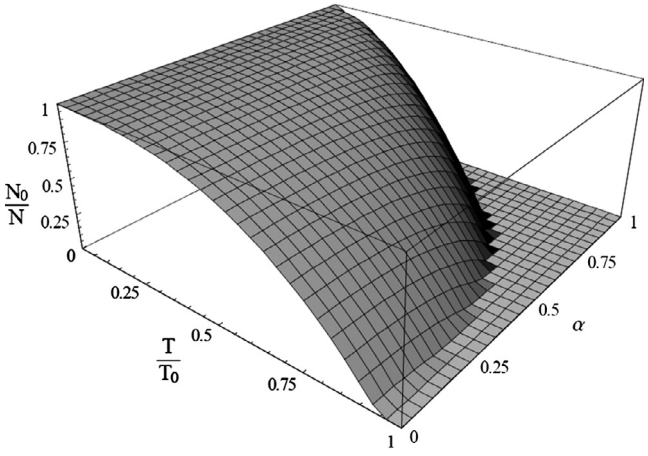

Fig. 15 The condensate fraction N_0/N as a function of the reduced temperature T/T_0 and the rotation ratio α.

The study of BEC in a rotating optical lattice was done in the atomic physics group by Abdel-Gany et al. [166]. The effective trapping potential V_{eff} for rotating optical lattice trap is considered to be,

$$V_{eff} = \frac{m}{2}\left[\omega_z^2 z^2 + \omega_\perp^2 r_\perp^2\right] + V_0\left[sin^2\left(\frac{\pi x}{d}\right) + sin^2\left(\frac{\pi y}{d}\right)\right] - \frac{m}{2}\Omega^2 r_\perp^2 \tag{34}$$

where d is the lattice spacing. The dependence of the condensate fraction, critical temperature, and the heat capacity on the recoil frequency, optical potential depth, and rotating frequency is investigated. The results show that the normalized recoil frequency can control the characteristic shape of the condensate fraction Fig. 16. Furthermore, our results show that the rotating BEC in optical lattice is accompanied by a peak in the critical temperature T_c at defined value for the normalized recoil frequency $S_\perp$, Fig. 17. This remarkable behavior was observed experimentally by Burger et al. [167] and numerically detected for non-rotating boson gas in optical lattice by Blakie et al. [168].

Bose–Einstein condensates in optical lattices represent model systems for solid state physics with yet unprecedented level of control. They can be used for exploring a wide range of fundamental problems in condensed matter physics such as Mott (metal-insulator) transitions, Anderson localization, type II superconductivity, and quantum Hall effect.

Exactly solvable models are very important in physics since they enable physicists to estimate the accuracy of the different approximate methods. In condensed atomic systems, the major problem involves solving many body interacting systems. The group of atomic physics at the Physics Department of the Faculty of Science – Cairo University has started to work on an exactly solvable model for a system composed of two species of identical Bosons in three-dimensional space interacting via harmonic potential. Aboul-Seoud et al. [169] have studied a system of two N-particles of identical Bosons with equal numbers, assuming that particles belonging to the same species repel each other and particles belong to different species attract each other. It was realized that the system is condensed in one channel when the coupling strengths are identical and in two channels when the coupling strengths are different. This study will enable us to understand the behavior of the miscibility of

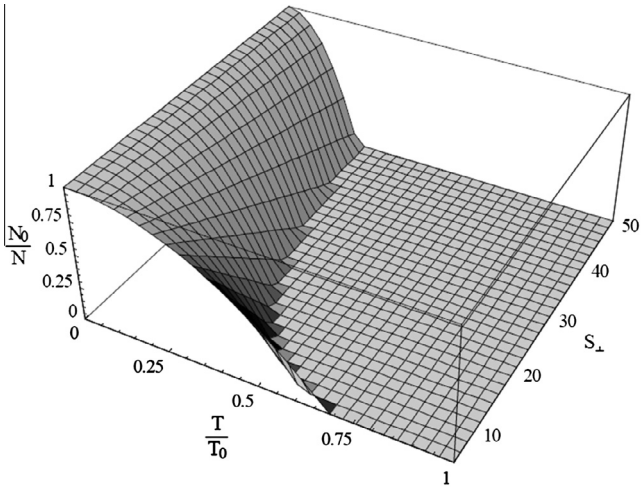

Fig. 16 The condensate fraction N_0/N as a function of the normalized recoil frequency S and the reduced temperature T/T_0 .

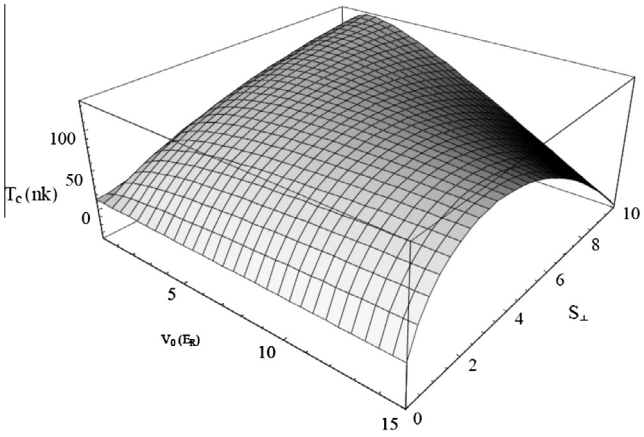

Fig. 17 The normalized recoil frequency S as function of the critical temperature T_c and the optical depth V_0.

atomic species as a function of the variations in the coupling strengths between the Bose species.

Further research activities in the field of BEC are being pursued by members of our atomic physics group. The research focuses on the study of the thermodynamics of Bose systems at finite temperature and inter-particle interactions. A system of equations describes trapped and condensed Bose systems at finite temperature is being investigated. The description of weakly interacting Bosons at zero temperature saw a breakthrough in 1947 with the seminal work of Bogoliubov [170], who derived the mean field equations that govern the statics, as well as the dynamics, of the condensed state. Bogoliubov's work correctly describes the microscopic low energy spectrum of the condensed state of a uniform condensate. Further progress was achieved through the work of Gross and Pitaevskii [171,172], who derived the zero temperature equations of a non-uniform condensate. Their approach has become the basis for much of the theoretical work on degenerate Bose gases. This work saw a surge of activity after the experimental realization of Bose–Einstein Condensation in electromagnetic-optical traps containing metastable vapors of alkali atoms [144,145].

More work is needed, however, to address both dynamical and thermodynamic aspects of the condensed phase at finite temperatures. At finite temperature, the system contains bosonic quasi-particle excitations. As the temperature is raised, the density of such excitations increases and their interactions with the condensate particles, as well as among themselves, may have a pronounced effect on the physics of the trapped system. Another aspect comes about because of the experimental possibility to fine-tune the inter-particle interactions using Feschbach resonances. This means that the interactions between the atoms in the condensate are not weak anymore. The validity of many of the approaches that have been developed with both finite temperature and strong inter-particle interactions has been questioned by Yukalov [173]. In order to treat these effects consistently, he derived a system of coupled equations for the main quantities that govern the macroscopic properties of degenerate trapped gases. These quantities include the condensate density, the density of non-condensate particles, the local speed of sound, and the anomalous density of the trapped system. We are comparing the solutions we are obtaining with known experimental results [174]. This approach is promising since it appears that it can be

easily generalized to include non-uniformities due to vortices or other special excitations, as well as dynamic phenomena at finite temperature. The results of our work are currently being prepared for submission for publication.

Concluding, I would like once more to stress that this review article was by no means an attempt to cover the whole of developments of atomic physics of the last half century. Rather, it was aimed at outlining the contributions of the atomic physics group of Cairo University that I had the honor to lead for the past four decades, as well as the research work I conducted during my scientific visits to the FOM-Institute for Atomic and Molecular Physics in Amsterdam.

With future publications, our group hopes to continue participating in the worldwide edifice of atomic physics.

Conflict of interest

The author has declared no conflict of interest.

Compliance with Ethics Requirements

This article does not contain any studies with human or animal subjects.

References

[1] Ramsauer C, Kollath R. Uber den wirkungsquerschnitt der edelgasmolek ule gegen uber elektronen unterhalb. Ann Phys 1929;3:536–64.

[2] Ramsauer C, Kollath R. Die winkelverteilung bei der streuung langsamer elektronen an gasmolekülen. II. Fortsetzung. Ann Phys 1932;12:529–61.

[3] Tate JT, Smith PT. Ionization potentials and probabilities for the formation of multiply charged ions in the alkali vapors and in krypton and xenon. Phys Rev 1934;46:773–6.

[4] Bleakney W, Smith LG. The ionization probability of He^{++}. Phys Rev 1936;49:402–12.

[5] Hughes AL, Rojansky V. On the analysis of electronic velocities by electrostatic means. Phys Rev 1929;34:284–90 [Phys Rev 1929;34:284].

[6] Massey HSW, Smith RA. The passage of positive ions through gases. Proc Roy Soc 1933;A142:142–72.

[7] Stueckelberg EC. Theorie der unelastischen Stösse zwischen Atomen. Helv Phys Acta 1932;5:370–422.

[8] Landau LD. On the theory of transfer of energy at collisions II. Z Phys Sov Un 1932;2:46–51.

[9] Zener C. Non-adiabatic crossing of energy levels. Proc Roy Soc 1932;A137:696–702.

[10] Massey HSW, Burhop EHS. Electronic and ionic impact phenomena. Oxford: The Clarendon Press; 1952.

[11] Fox RE. Multiple ionization in argon and krypton by electron impact. J Chem Phys 1960;1960(33):200–5.

[12] Fayard F. Energy dependence for single and double ionization by electron impact between 250 and 2200 eV. J Chem Phys 1968;48:478–87.

[13] Van der Wiel MJ, EL-Sherbini ThM, Vriens L. Multiple ionization of He, Ne and Ar by 2–16 keV electrons. Physica 1969;42:411–20.

[14] El-Sherbini ThM, Van der Wiel MJ, De Heer FJ. Multiple ionization of Kr and Xe by 2–14 keV electrons. Physica 1970;48:157–64.

[15] Van der Wiel MJ. Small-angle scattering of 10 keV electrons in He, Ne, and Ar. Physica 1970;40:411–24.

[16] Bethe HA, Rose ME, Smith LP. The multiple scattering of electrons. Proc Am Philos Soc 1938;78:573–85.

[17] Krause MO, Carlson TA. Vacancy cascade in the irradiation of atoms with photons. Phys Rev 1967;158:18–24.

[18] Cairns RB, Harrison H, Schoen RI. Multiple photoionization of xenon. Phys Rev 1969;183:52–9.

[19] El-Sherbini ThM, Van der Wiel MJ. Oscillator strengths for multiple ionization in the outer and first inner shells of Kr and Xe. Physica 1972;62:119–38.

[20] Samson JAR. The measurements of the photo-ionization cross sections of the atomic gases. Adv Atom Mol Phys 1966;2:177–260.

[21] Amusia MYa, Cherepkov NA, Chernysheva LV. Cross sections for the photo-ionization of noble gas atoms with allowance of multi-electron correlations. Sov Phys – JETP 1971;33:90–6.

[22] Wendin G. Collective resonance in the $4d^{10}$ shell in atomic Xe. Phys Lett A 1971;37:445–6.

[23] Van der Wiel MJ, El-Sherbini ThM, Brion CE. K shell excitation of nitrogen and carbon monoxide by electron impact. Chem Phys Lett 1970;7:161–4.

[24] El-Sherbini ThM, Van der Wiel MJ. Ionization of N_2 and CO by 10 keV electrons as a function of the energy loss I. Valence electrons. Physica 1972;59:433–52.

[25] Van der Wiel MJ, El-Sherbini ThM. Ionization of N_2 and CO by 10 keV electrons as a function of the energy loss II. Inner-shell electrons. Physica 1972;59:453–62.

[26] Bates DR. Atomic and molecular processes. London: Acad Press; 1962, p. 549.

[27] Merzbacher E. Quantum mechanics. 2nd ed. John Wiley & Sons, Inc; 1970. p. 450–4.

[28] Hasted JB. Inelastic collisions between ions and atoms. Proc Roy Soc Lond 1952;212A:235–48.

[29] Hasted JB. Advances in electronics, vol. XIII. New York: Academic Press; 1960.

[30] Morgan GH, Everhart E. Measurements of inelastic energy loss in large-angle Ar^+ on Ar collisions at keV energies. Phys Rev 1962;128:667–76.

[31] Kessel QC, Everhart E. Coincidence measurements of large-angle Ar^+ on Ar collisions. Phys Rev 1966;146:16–27.

[32] Niehaus A, Ruf M. An experimental study of autoionization processes occurring in $2\,eV^{-1}$ keV He^{2+}–Hg collisions. I. Electron and ion energy spectra. J Phys B: Atom Mol Phys 1976;9:1401–18.

[33] Winter H, Bloemen E, De Heer FJ. VUV radiation, slow ions and electrons produced in collisions of multiply charged Ne ions with He and Ar. J Phys B: Atom Mol Phys 1977;10: L599–604.

[34] Winter H, El-Sherbini ThM, Bloemen E, De Heer FJ, Salop A. A comparison between radiative and non-radiative de-excitation after electron capture by multiply charged ions. Phys Lett 1978;68A:211–4.

[35] Fano U, Lichten W. Interpretation of Ar^+–Ar collisions at 50 KeV. Phys Rev Lett 1965;14:627–31.

[36] Woerlee PH, El-Sherbini ThM, De Heer FJ, Saris FW. Energy spectra of electrons produced in collisions of multiply charged neon ions with noble-gas atoms. J Phys B: Atom Mol Phys 1979;12:L235–41.

[37] Kishinevskii LM, Parilis ES. Auger ionization of atoms by mutiply-charged ions. Model of two coulomb centers. Sov Phys – JETP 1969;28:1020–34.

[38] El-Sherbini ThM, Farrag A. Configuration interaction in the spectrum of Kr II. J Phys B: Atom Mol Phys 1976;9:2797–803.

[39] El-Sherbini ThM, Salop A, Bloemen E, De Heer FJ. Target dependence of excitation resulting from electron capture in collisions of 200 keV $Ar6^+$ ions with noble gases. J Phys B: Atom Mol Phys 1979;12:L579–82.

[40] El-Sherbini ThM, Salop A, Bloemen E, De Heer FJ. Excitation and ionization resulting from electron capture in $Ar^{6+} + H_2$ collisions at ion projectile energies of 200–1200 keV. J Phys B: Atom Mol Phys 1980;13:1433–49.

[41] El-Sherbini ThM, ed. In: Proceedings of arab symposium on atomic and molecular processes in controlled thermonuclear fusion research, Cairo University 14–18 November, 1988.
[42] El-Sherbini ThM, De Heer FJ. Projectile excitation in the collision of Ar^{q+} (q = 1, 2 and 3) with He and Ne. J Phys B: Atom Mol Phys 1982;15:423–38.
[43] Garstang RH. Some line strengths for ionized neon. Monthly Not Roy Astron Soc 1950;110:612–4.
[44] Garstang RH. Transition probabilities of forbidden lines. J Res Nat Bur Stand, Sec A 1964;68:61–74.
[45] Wiese WL, Smith MW, Miles BM. Atomic transition probabilities. 1969 Nat Bur Stand NSRDS-NBS4; 1969.
[46] Luyken BFJ. Transition probabilities and radiative lifetimes for Ne II. Physica 1971;51:445–60.
[47] Luyken BFJ. Transition probabilities and radiative lifetimes for Ar II. Physica 1972;60:432–66.
[48] El-Sherbini ThM. Calculation of transition probabilities and radiative lifetimes for singly ionized krypton. J Phys B: Atom Mol Phys 1975;8:L183–4.
[49] El-Sherbini ThM. Calculation of Xe II line strengths and radiative lifetimes in intermediate coupling. Z Phys 1975;A275:1–3.
[50] El-Sherbini ThM. Line strengths and lifetimes for Kr II. Z Phys 1976;A276:325–7.
[51] Aymar M, Crance M, Klapisch M. Results of parametric potential applied to rare gases. J Phys 1970;31:141–8.
[52] Minnhagen L, Strihed H, Petarsson B. Revised and extended analysis of singly ionized krypton, Kr II. Ark Fys 1968;39:471–93.
[53] El-Sherbini ThM, Zaki MA. Perturbations in the $5p^4 6s$ and $5p^4 5d$ configurations of Xe II. J Phys B: Atom Mol Phys 1978;11:2061–8.
[54] El-Sherbini ThM. Transition probabilities and radiative lifetimes for singly ionized xenon. J Phys B: Atom Mol Phys 1976;9:1665–71.
[55] El-Sherbini ThM. Configuration interaction in the spectrum of singly ionized xenon. In: Proceedings of the X international conference on the physics of electronic and atomic collisions (ICPEC), Paris 21–27 July 1977.
[56] El-Sherbini ThM. Excitation mechanisms in the singly ionized krypton laser. Phys Lett 1982;88A:169–71.
[57] Serrao JM. The absorption spectrum of beryllium. J Quant Spectrosc Radiat Transfer 1985;3:219–26.
[58] El-Sherbini ThM, Mansour H, Farrag A. Hartree–Fock energies of the doubly excited states of the boron isoelectronic sequence. Ann Phys 1987;44:419–22.
[59] Martinson I, Curtis LJ. Spectroscopic studies of the structure of *highly ionized atoms*. Cont Phys 1989;30:173–85.
[60] Norreys P, Zhang J, Cairns G, Djaoui A, Dwivedi L, Key M, et al. Measurement of the photo-pump strength of the 3d–5f transitions in the automatically line matched Ni-like Sm photo-pumped X-ray laser. J Phys B: Atom Mol Opt Phys 1993;26:3693–9.
[61] Nilson J. Lasing on the 3d–3p neon like X-ray laser transitions driven by a self-photo-pumping mechanism. Phys Rev A 1996;53:4539–47.
[62] Mathews DL, Hagelstein PL, Rosen MD, Echart MJ, Ceglio NM, Hazi AU, et al. Demonstration of a soft X-ray amplifier. Phys Rev Lett 1985;54:110–3.
[63] Hagelstein PL, Basv S, Muendel MH, Bravd JP, Tavber D, Kavshik S, et al. The MIT short-wavelength laser project: a status report. In: Proceedings of the international colloquium on X-ray laser, vol. 116, York, United Kingdom; 1990. p. 255–62.
[64] Jaegle P, Jamelot G, Carillon A, Wehenkel C. Soft-X-ray amplification by lithiumlike ions in recombining hot plasmas. Jpn J Appl Phys 1987;17:563–74.
[65] Silfvast WT, Wood OR. Photoionization lasers pumped by broadband soft-X-ray flux from laser-produced plasmas. J Opt Soc Am 1987;B4:609–18.
[66] Jaegle P, Jamelot G, Carillon A, Klisnick A, Sureau A, Guennou H. Hot plasmas. J Opt Soc Am 1987;B4:563–74.
[67] Krishnan M, Trebes J. Design considerations for optically pumped, quasi-cw, uv and xuv lasers in the Be isoelectronic sequence. Am Ins Phys 1984;46:514–27.
[68] Feldman U, Seely JF, Bhatia AK. Density sensitive X-ray line ratios in the Be I, B I and Ne I isoelectronic sequences. J Appl Phys 1985;58:3953–7.
[69] Al-Rabban MM. Electron excitation in the beryllium-isoelectronic sequence and X-ray laser. MSc thesis, Faculty of Science, Ain Shams University; 1995.
[70] Hibbert A. CIV3 – A general program to calculate configuration interaction wave functions and electric-dipole oscillator strengths. Comput Phys Commun 1975;9:141–72.
[71] Friedrich H. Theoretical atomic physics. Springer Verlag; 1991.
[72] Yahia ME, Azzouz IM, Allam SH, El-Sherbini ThM. Laser gain by electron collisional pumping of Ar VII–V XII. Opt Laser Technol 2008;40:1008–17.
[73] Elton RC. X-ray lasers. Academic Press INC; 1990.
[74] Vriens L, Smeets A. Cross-section and rate formulas for electron-impact ionization, excitation, deexcitat and total depopulation of excited atoms. Phys Rev 1980;A22:940–51.
[75] Allam SH. CRMO-Collisional Radiative Model. Computer Code, Private Communication; 2005
[76] Palumbo LJ, Elton RC. Short-wavelength laser calculations for electron pumping in carbonlike and heliumlike ions. J Opt Soc Am 1977;67:480–8.
[77] El-Sherbini ThM, Wahby AS. Energy levels of the single excited states in He I isoelectronic sequence. Proc Ind Natl Sci Acad 1990;56A:39–46.
[78] El-Sherbini ThM, Al-Rabban MM. Soft X-ray laser transitions in the Be-isoelectronic sequence. In: Proceedings of the 2nd international conference on lasers and applications, Cairo University 16–19 September 1996. p. 86–9.
[79] El-Sherbini ThM, Farrag AA, Mansour HM, Rahman AA. Electrical dipole oscillator strengths and radiative lifetimes in the boron isoelectronic sequence. Ann Phys 1987;44:412–8.
[80] El-Sherbini ThM, Mansour HM, Farrag AA, Rahman AA. Energy levels of the single excited states in the boron isoelectronic sequence. Ann Phys 1989;46:105–12.
[81] El-Sherbini ThM, Al-Rabban MM. Laser transitions in the boron-like ions of NIII, OIV and FV. Infrared Phys 1991;31:595–7.
[82] Allam SH, Farrag AA, Refaie AI, El-Sherbini ThM. Oscillator strengths of allowed transitions for CI-isoelectronic sequence. Arab J Nucl Sci Appl 1999;32:89–95.
[83] El-Sherbini ThM, Farrag AA. Core-excited doublet and quartet states in the sodium isoelectronic sequence. J Quant Spectrosc Radiat Transfer 1991;46:473–5.
[84] Younis WO, Allam SH, El-Sherbini ThM. Fine-structure calculations of energy levels, oscillator strengths, and transition probabilities for sodium-like ions (Co XVII–Kr XXVI). Atom Nucl Data Tables 2006;92:187–205.
[85] Younis WO, Allam SH, El-Sherbini ThM. Rate coefficients for electron impact excitation, de-excitation and laser gain calculations of the excited ions Co XVII up to Br XXV. Can J Phys 2010;88:257–69.
[86] El-Sherbini ThM, Rahman AA. Auto-ionizing states in Mg I. Ann Phys 1982;39:333–7.
[87] El-Sherbini ThM, Mansour HM, Farrag AA, Rahman AA. Electric dipole oscillator strength and radiative lifetimes in the magnesium isoelectronic sequence. Ann Phys 1988;45:498–506.
[88] El-Sherbini ThM, Mansour HM, Farrag AA, Rahman AA. Energy levels of the single excited states in the magnesium isoelectronic sequence. Ann Phys 1989;46:144–8.
[89] Younis WO, Allam SH. Relativistic energy levels and transition probabilities for Al-like ions (Z = 33–35). Int Rev Phys 2011;5:207–46.

[90] El-Maaref AA, Uosif MA, Allam SH, El-Sherbini MTh. Energy levels, oscillator strengths and transition probabilities for Si-like P II, S III, Cl IV, Ar V and K VI. Atom Data Nucl Data Tables 2012;98:589–615.
[91] El-Maaref AA, Allam SH, Uosif MA, El-Sherbini ThM. The 4d–4p transition and soft X-ray laser wavelengths in Si-like ions. Can J Phys 2013;91:1–13.
[92] El-Maaref AA, Allam SH, El-Sherbini ThM. Energy levels, oscillator strengths and radiative rates of Si-like Zn XVII, Ga XVIII, Ge XIX and As XX. Atom Data Nucl Data Tables 2013 [in press].
[93] El-Maaref AA, Ahmed M, Allam SH. Fine-structure calculations of energy levels, oscillator strengths and transition probabilities for sulfur-like Fe XI. Atom Data Nucl Data Tables 2013 [in press].
[94] Lamia MA. Laser transitions in neutral potassium and potassium like ions, MSc thesis, Faculty of Science, Benha University; 2009.
[95] Refaie AI, El-Sharkawy H, Allam SH, El-Sherbini ThM. Theoretical electron impact excitation, ionization and recombination rate coefficients and level population densities for scandium-like ions. Int J Pure Appl Phys 2007;3:75–82.
[96] Abdelaziz WS, El-Sherbini ThM. Reduced population and gain coefficient calculations for soft X-ray laser emission from Eu^{35+}. Opt Laser Technol 2010;42:699–702.
[97] Tognoni E, Palleschi V, Corsi M, Cristoforetti G. Quantitative micro-analysis by laser-induced breakdown spectroscopy: a review of the experimental approaches. Spectrochim Acta 2002;B57:1115–30.
[98] Barrette L, Turmel S. On-line iron-ore slurry monitoring for real-time process control of pellet making processes using laser-induced breakdown spectroscopy: graphitic vs. total carbon detection. Spectrochim Acta 2001;B56:715–23.
[99] Hassan M, Sighicelli M, Lai A, Colao F, Ahmed AH, Fantoni R, et al. Studying the enhanced phytoremediation of lead contaminated soils via laser induced breakdown spectroscopy. Spectrochem Acta 2008;B63:1225–9.
[100] Abdel-Salam Z, Al Sharnoubi J, Harith MA. Qualitative evaluation of maternal milk and commercial infant formulas via LIBS. Talanta 2013;115:422–6.
[101] St-Onge L, Kwong E, Sabsabi M, Vadas E. Rapid analysis of liquid formulations containing sodium chloride using laser-induced breakdown spectroscopy. J Pharm Biomed Anal 2004;36:277–84.
[102] Narayanan V, Thareja R. Emission spectroscopy of laser-ablated Si plasma related to nanoparticle formation. Appl Surf Sci 2004;222:382–93.
[103] Garc'ya-Ayuso L, Amador-Hernandez J, Fernandez-Romero J, De Castro M. Characterization of jewellery products by laser-induced breakdown spectroscopy. Anal Chim Acta 2002;457:247–56.
[104] Capitelli F, Colao F, Provenzano M, Fantoni R, Brunetti G, Senesi N. Determination of heavy metals in soils by laser induced breakdown spectroscopy. Geoderma 2002;106:45–62.
[105] Galmed AH, Kassem AK, Von Bergmann H, Harith MA. A study of using femtosecond LIBS in analyzing metallic thin film – semiconductor interface. Appl Phys 2011;B102:197–204.
[106] Khedr A, Papadakis V, Pouli P, Anglos D, Harith MA. The potential use of plume imaging for real-time monitoring of laser ablation cleaning of stonework. Appl Phys 2011;B105:485–92.
[107] Colao F, Fantonia R, Lazica V, Paolinia A, Fabbria F, Orib G, et al. LIBS feasibility for in situ planetary exploration: an analysis on Martian rock analogues. Planet Space Sci 2004;52:117–23.
[108] Sanchez-Ake C, Bolanos M, Ramirez C. Emission enhancement using two orthogonal targets in double pulse laser-induced breakdown spectroscopy. Spectrochim Acta Part B: Atom Spectrosc 2009;64:857–62.
[109] Cristoforetti G, Legnaioli S, Pardini L, Palleschi V, Salvetti A, Tognoni E. Spectroscopic and shadow-graphic analysis of laser induced plasmas in the orthogonal double pulse pre-ablation configuration. Spectrochim Acta Part B: Atom Spectrosc 2006;61:340–50.
[110] Piepmeier EH, Malmstadt HV. Q-switched laser energy absorption in the plume of an aluminum alloy. Anal Chem 1969;41:700–7.
[111] Sattmann R, Sturm V, Noll R. Laser-induced breakdown spectroscopy of steel samples using multiple Q-switch Nd:YAG laser pulses. J Phys D: Appl Phys 1995;28:2181–7.
[112] Petukh ML, Rozantsev VA, Shirokanov AD, Yankovskii AA. The spectral intensity of the plasma of single and double laser pulses. J Appl Spectrosc 2000;67:1097–101.
[113] St-Onge L, Detalle V, Sabsabi M. Enhanced laser-induced breakdown spectroscopy using combination of fourth-harmonic and fundamental Nd:YAG pulses. Spectrochim Acta B: Atom Spectrosc 2002;57:121–35.
[114] Noll R. Laser induced breakdown spectroscopy. Berlin-Heidelberg: Springer Verlag; 2012.
[115] Tarasenko NV, Burakov VS, Butsen AV. Laser ablation plasmas in liquids for fabrication of nanosize particles. In: VI serbian–belarusian symp on phys and diagn of lab & astrophys plasma, vol. 82, Belgrade, Serbia, 22–25 August 2006, Pub Astron Obs Belgrade, 2007. p. 201–11.
[116] Griem HR. Plasma spectroscopy. McGraw-Hill Inc.; 1964.
[117] Griem HR. Spectral line broadening by plasmas. New York: Academic Press; 1974.
[118] Hegazy H, Sharkawy H, El-Sherbini ThM. Use of spectral lines of pure Ti target for the spectroscopic diagnostics of the laser induced plasma in vacuum. Proc AIP Conf 2007;888:152–9.
[119] El-Sherbini AM, Abdel Hamid A, El-Sherbini ThM. Collisional-radiative model for neutral argon plasma. In: Proceedings of the XXVth international conference on solid state physics and materials science, Luxor 6–10 March, 2005. p. 14–18.
[120] El-Sergany F, Atta Khedr M, Abuzeid H, Montasir M, El-Sherbini ThM. Elemental analysis of some minerals using the laser induced plasma spectroscopy. In: Proceedings of the first Euro-mediter symposium, Cairo 2–6 November, 2000. p. 14–7.
[121] El-Sherbini AM, Hegazy H, El-Sherbini ThM, Cristoforretti G, Legnaioli S, Palleschi V, et al. Evaluation of self-absorption coefficients of aluminum emission lines in laser-induced breakdown spectroscopy measurements. Spectrochim Acta Part B: Atom Spectrosc 2005;60:1573–9.
[122] El-Sherbini AM, Hegazy H, El-Sherbini ThM. Measurement of electron density utilizing the H_α-line from laser produced plasma in air. Spectrochim Acta Part B: Atom Spectrosc 2006;61:532–9.
[123] El-Sherbini AM, El-Sherbini ThM, Hegazy, Cristoforetti G, Leganaioli S, Pardini L, et al. Measurement of the Stark broadening coefficient of atomic emission lines by laser-induced breakdown spectroscopy technique. Spectrosc Lett 2007;40:643–58.
[124] El-Sherbini AM, Refaie AI, Aboulfotouh AM, El-Kamhawy AA, Abdel Sabour K, Imam H, et al. An assessment of LIBS-diagnostics of plasma using the hydrogen Hα-line at different laser energies. In: Proceedings of the third arab international conference on physics and materials science, Alexandria 21–23 October, 2009. p. 176–87.
[125] El-Sherbini AM, Aboulfotouh AM, Allam SH, El-Sherbini ThM. Diode laser absorption measurements at the H_α-transition in laser induced plasmas on different targets. Spectrochim Acta Part B: Atom Spectrosc 2010;65:1041–6.
[126] El-Sherbini AM, Al Amer AS, Hassan AT, El-Sherbini ThM. Measurements of plasma electron temperature utilizing magnesium lines appeared in laser produced aluminum plasma in air. Opt Photon J 2012;2:278–85.

[127] El-Sherbini AM, Al Amer AS, Hassan AT, El-Sherbini ThM. Spectrometric measurement of plasma parameters utilizing the target ambient gas O I and N I atomic lines in LIBS experiment. Opt Photon J 2012;2:286–93.
[128] Hegazy H, Allam SH, Chaurasia S, Dhareshwar L, El-Sherbini ThM, Kunze HJ, et al. Joint experiments on X-ray/particle emission from plasmas produced by laser irradiating nano structured targets. Am Inst Phys Plasma Fusion Sci 2008;996:243–50.
[129] El-Sherbini AM, Aboulfotouh AM, Rashid FF, Allam SH, El-Dakrouri A, El-Sherbini ThM. Observed enhancement in LIBS signals from nano vs. bulk targets: comparative study of plasma parameters. World J Nano Sci Eng 2012;2:181–8.
[130] Hegazy H, Abdel-Rahim FM, Allam SH. Evolution of Al plasma generated by Nd-Yag laser radiation at the fundamental wavelength. Appl Phys B 2012;108:665–73.
[131] Hegazy H, Abdel-Ghany HA, Allam SH, El-Sherbini ThM. Spectral evolution of nano-second laser interaction with Ti target in air. Appl Phys B 2013;110:509–18.
[132] Hermann J, Thomann AL, Boulmer-Leborgne C, Dubereuil B, De Giorgi ML, Perrone A, et al. Plasma diagnostics in pulsed laser TiN layer deposition. J Appl Phys 1995;77:2928–36.
[133] Einstein A. On the quantum theory of radiation. Phys Z 1917;18:121–8.
[134] Phillips W, Metcalf H. Laser deceleration of an atomic beam. Phys Rev Lett 1982;48:596–9.
[135] Prentiss M, Cable A. Slowing and cooling an atomic beam using an intense optical standing wave. Phys Rev Lett 1989;62:1354–7.
[136] Metcalf H, Van der Straten P. Laser cooling and trapping of neutral atoms. Phys Rep 1994;244:203–86.
[137] Prodan J. Stopping atoms with laser light. Phys Rev Lett 1985;54:992–5.
[138] Hansch TW, Schawlow AL. Cooling of gases by laser radiation. Opt Commun 1975;13:68–9.
[139] Chu S, Hollberg L, Bjorkholm JE, Cable A, Ashkin A. Three-dimensional viscous confinement and cooling of atoms by resonance radiation pressure. Phys Rev Lett 1985;55:48–51.
[140] Pethick CJ, Smith R. Bose–Einstein condensation in dilute gases. Cambridge University Press; 2002.
[141] Hess HF. Evaporative cooling of magnetically trapped and compressed spin-polarized hydrogen. Phys Rev B 1986;34:3476–9.
[142] Ketterle W. When atoms behave as waves: Bose–Einstein condensation and the atom laser. Rev Mod Phys 2002;74:1131–51.
[143] Molenear PA, Van der Straten P, Heideman HG. Diagnostic technique for Zeeman-compensated atomic beam slowing: technique and results. Phys Rev A 1997;55:605–14.
[144] Anderson MH, Ensher JR, Matthews MR, Wieman CE, Cornell EA. Observation of Bose–Einstein condensation in a dilute atomic vapor. Science 1995;269:198–201.
[145] Davis KB, Mewes MO, Andrews MR, Van Druten NJ, Durfee DS, Kurn DM, et al. Bose–Einstein condensation in a gas of sodium atoms. Phys Rev Lett 1995;75:3969–73.
[146] Bradley CC, SAckett CA, Hulet RG. Bose–Einstein condensation of lithium: observation of limited condensate number. Phys Rev Lett 1997;78:985–9.
[147] Greiner M, Regal C, Jin D. Emergence of a molecular Bose–Einstein condensate from a Fermi gas. Nature 2003;426:537–40.
[148] Bloch I. Ultracold quantum gases in optical lattices. Nat Phys 2005;1:23–30.
[149] El-Sherbini ThM. Bose–Einstein condensation. Proc Am Inst Phys Conf 2004;748:44–54.
[150] Bagnato V, Pritchard DE, Kleppner D. Bose–Einstein condensation in an external potential. Phys Rev A 1987;35:4354–8.
[151] Ketterle W, Van Druten NJ. Bose–Einstein condensation of a finite number of particles trapped in one or three dimensions. Phys Rev A 1996;54:656–60.
[152] Dalfovo F, Giorgini S, Pitaevskii LP, Stringari S. Theory of Bose–Einstein condensation in trapped gases. Rev Mod Phys 1999;71:463–512.
[153] Kirsten K, Toms DJ. Bose–Einstein condensation in arbitrarily shaped cavities. Phys Rev E 1999;59:158–67.
[154] Hassan AS, El-Badry AM. Critical points of a three-dimensional harmonically trapped Bose gas. Physica B 2009;404:1947–50.
[155] Williams RA, Al-Assam S, Foot CJ. Observation of vortex nucleation in a rotating two-dimensional lattice of Bose–Einstein condensates. Phys Rev Lett 2010;104:050404–7; Smith RP, Campbell RL, Tammuz N, Hadzibabic Z. Can a Bose gas be saturated? Phys Rev Lett 2011;106:230401–4.
[156] Hassan AS, El-Badry AM. Effective width and expansion energy of the interacting condensed 87Rb Bose gas with finite size effects. Turk J Phys 2009;33:21–30.
[157] Hassan AS. Effective area and expansion energy of trapped Bose gas in a combined magnetic–optical potential. Phys Lett A 2010;374:2106–12.
[158] Hassan AS, El-Badry AM, Soliman SS. Critical temperature of a Bose–Einstein condensate in a 3D non-cubic optical lattice. Physica B 2010;405:4768–71.
[159] Hassan AS, El-Badry AM, Soliman SS. Thermodynamic properties of a condensed Bose gas in a harmonic trap. Physica B 2013;410:63–7.
[160] Hassan AS, El-Badry AM, Soliman SS. Thermodynamic properties of a rotating Bose gas in harmonic trap. Eur Phys J D 2011;64:465–71.
[161] Hassan AS, El-Badry AM, Mohammedein AM, Ebeid MR. Effective widths of boson gas confined in a harmonic rotating trap. Phys Lett A 2012;376:1781–5.
[162] Bretin V, Stock S, Seurin Y, Dalibard J. Fast rotation of a Bose–Einstein condensate. Phys Rev Lett 2004;92:050403–6.
[163] Blanc X, Rougerie N. Lowest Landau level vortex structure of a Bose–Einstein condensate rotating in a harmonic plus quartic trap. Phys Rev A 2008;77:053615–22.
[164] El-Sherbini ThM, Hassan D, Galal AA, Hassan AS. Thermodynamic properties of a rotating Bose-Einstein condensation in a harmonic plus quartic trap. Eur Phys J 2013;67:185–91.
[165] Kling S, Pelster A. Thermodynamical properties of a rotating ideal Bose gas. Phys Rev A 2007;76:023609–14.
[166] Abdel-Gany HA, Ellithi AY, Galal AA, Hassan AS. Thermodynamic properties of a rotating Bose–Einstein condensation in a 2D optical lattice. Tuk J Phys 2014;38:39–49.
[167] Burger S, Cataliotti FS, Fort C, Madaloni P, Minardi F, Inguscio M. Quasi-2D Bose–Einstein condensation in an optical lattice. Eur Phys Lett 2002;57:1–6.
[168] Blakie PB, Bezett A, Buonsante PF. Degenerate Fermi gas in a combined harmonic-lattice potential. Phys Rev A 2007;75:053609–18.
[169] Aboul-Seod A, Hussein A, Galal AA, El-Sherbini ThM. An exactly solvable model of two species of identical bosons interacting via a harmonic oscillator potential. Phys Rev A 2013 [submitted for publication].
[170] Bogoliubov NN. On the theory of superfluidity. J Phys USSR 1947;11:23–32.
[171] Gross EP. Structure of a quantized vortex in boson systems. Nuovo Cimento 1961;20:454–7.
[172] Pitaevskii LP. Vortex lines in an imperfect Bose gas. Sov Phys JETP 1961;13:451–4.
[173] Yukalov VI. Bose–Einstein condensation and gauge symmetry breaking. Laser Phys Lett 2007;4:632–47.
[174] Gerbier F, Thywissen JH, Richard S, Hugbart M, Bouyer P, Aspect A. Critical temperature of a trapped, weakly interacting Bose gas. Phys Rev Lett 2004;92:030405–8.